Fabrication of Zinc Oxide Nanowire Arrays for use as Photoanodes in Dye-sensitized Solar Cells

A project report

submitted in partial fulfillment

of the requirements for the degree of

Master of Engineering

in the Faculty of Engineering

by

Anand Prakash

Department of Chemical Engineering

Indian Institute of Science

Bangalore 560012 (India)

May 2012

Abstract

Dye-sensitized solar cells (DSSCs) are promising photovoltaic devices for the generation of low cost, carbon free energy. Wide-bandgap semiconductor nanowire photoanodes have the potential to improve the efficiencies of DSSCs. The nanowires provide a direct conduction path for electron transport, and can improve current densities and efficiencies by an order of magnitude. Controlling and orienting the dimensions of the nanowires (i.e. nanowire height, diameter, and spacing) for DSSCs is vital for efficiency enhancement. The objective of this work is to utilize thermally-stable, ordered, gold nanoparticle arrays as templates to form vertically-ordered, zinc oxide nanowires with controlled spacing and diameter using the vapour liquid solid (VLS) growth technique, and test their utility as photoanodes in DSSCs. This report begins with an overview of the working principle of nanowire based DSSCs. The next section contains a brief literature review on generic nanoparticle synthesis. It is followed by discussion of various kinds of template methods including soft-lithography and self-assembly of nanoparticles for the preparation of metal catalyst arrays. The next part of the report gives an overview of the various kinds of growth modes observed for vertically aligned nanowires, with focus on specific experimental conditions for establishing VLS growth. The final section of the report focuses on the remaining challenges for realizing a nanowire array based DSSC.

Table of Contents

List of figures

1 Introduction

1.1 Background

The worldwide demand for energy is increasing exponentially day by day. The global energy problem is manifested by decreasing fossil fuel supplies and sky-high oil and gas prices. There is growing concern that the production of oil cannot keep up with growing energy demand. In addition, the combustion of fossil fuels causes emission of greenhouse gas, which leads to global temperature rise. The development of carbon-free sources of energy has become one of the main scientific challenges of this century[1].

Sunlight is an ideal source of energy which is readily available. It seems to be the most viable choice to meet clean energy demand. The current rate of energy need is 13 TW while the sun continuously delivers 120,000 TW to the earth[1]. Hence, the present energy requirement can be satisfied by covering only 0.1% of the earth's surface using 10% efficient solar cells[2]. While developed technologies are efficient to harness solar energy, they are not an economically viable alternative to fossil fuels[3]. The major barrier for the large-scale application of solar power is the high cost of existing solar cells. Therefore, there is a need of innovations to make efficient and cost-effective version of photovoltaic cells.

1.2 Excitonic solar cell

Among the different emerging photovoltaic options, excitonic solar cells (XSCs) have been garnering attention for last two decades and have emerged as promising route to inexpensive solar cells. In a photovoltaic cell, the steps required to convert light to electricity are photon absorption, exciton creation, exciton separation to free carriers and carrier collection by the electrodes. The mechanism of photoconversion in XSCs differs from that in conventional silicon solar cells. In conventional silicon solar cells based on the p-n junction, light absorption, charge generation, charge separation and charge transport are coupled, and all take place in the same material. Consequently, in these conventional solar cells, electrons travel through hole rich regions of the cell and holes travel through electron rich regions. In contrast, in XSCs, the key solar-to electric energy processes are decoupled and exciton dissociation takes place at the interface between the constituent semiconductors. The main driving force for charge separation is an electro-chemical potential difference across the cell that leads to the photovoltaic effect. As a consequence, the electrons are transported through electron-rich materials and the holes are transported through hole-rich materials. Thus, XSCs encompass photovoltaic systems largely dependent on interfacial processes and so less expensive compounds can be used. On the other hand, conventional solar cell relies on crystallinity of materials for photovoltaic response, and requires highly crystalline and chemically pure materials. The production cost of such materials is unusually high which makes conventional solar cells expensive to produce. In addition, flexible substrates can be used for XSCs. These flexible substrates can be manufactured by roll-to-roll processing and hence cost of XSCs can be potentially reduced further.

Nanowires of wide bandgap semiconductor such as ZnO can act as the electron acceptor and conductor in XSC. The nanowire geometry provides a high interfacial area for light absorption and charge separation as well as faster electron transport for conduction. They have the potential to increase the overall efficiency. The reasons behind preferring ZnO nanowires in XSCs over other semiconductors are discussed later. However, nanowires in XSCs will be effective only with controlled and tailored dimensions and morphology (i.e., height, diameter, spacing and planar density). Fundamental and detailed understandings of the nanowire growth mechanism are required to have control over the process. With these objectives in mind, this project focuses on fabrication of the ZnO nanowire arrays on various substrates using the vapour-liquid-solid mechanism.

1.3 Dye-sensitized solar cell

Dye-sensitized solar cells are next-generation solar cells based on innovative technology with laboratory power conversion efficiencies over 11%[4]. Unlike conventional silicon-based solar cells, dye-sensitized solar cells consist primarily of a photosensitive dye at an interface of electron and hole collectors. The DSSC comprises of an electrolyte sandwiched between a photoanode and a catalytic-electrode (counter electrode). The photoanode is a nanoparticle film of wide gap semiconductor (typically ZnO or TiO_2) deposited on a transparent conducting oxide (TCO) glass substrate. A monolayer of dye molecules is adsorbed onto these nanocrystals. This configuration provides a large area at the semiconductor-dye-electrolyte interface for efficient cell operation.

A schematic presentation of energy levels of cell components is shown in **Figure 1.**. An incident photon is absorbed by the dye molecule, and an electron from the highest occupied molecular orbital (HOMO) is excited to the lowest unoccupied molecular orbital (LUMO). Excited electron at LUMO level is injected into the conduction band of the semiconductor nanoparticles at interface, leaving the dye molecule in an oxidised state. The injected electron percolates through the nanocrystalline structure to the photoanode and finally through an external load to the counter electrode. At the counter electrode, two electrons are transferred to the triiodide (I_3^-) in the electrolyte to yield iodide (I^-). The dye is regenerated by electron donation from the iodide, thereby closing the circuit. The regeneration of the sensitizer by iodide prevents the recapture of the conduction band electron by the oxidized dye. As shown in **Figure 1.**, the maximum open circuit voltage is the difference between the semiconductor's quasi-Fermi level and the Nernstian potential of the redox mediator. The carriers accumulate steadily at the dye-semiconductor–electrolyte interface and produce chemical potential across the cell which acts as the driving force for the carrier transport through the nanoparticle film.

Following the pioneering work of Graetzel and O'Regan[5] in 1991, the DSSCs have received much attention as an economical energy conversion device. They made the significant breakthrough by changing the morphology of the wide bandgap semiconductor from a smooth surface to a TiO_2nanoparticle film. This proved to be the key factor for a substantial increase in efficiency. The modified morphology provided the large surface area needed for enough dye to be adsorbed which in turn, increased light absorption efficiency of the cell. Subsequent work by various research groups have pushed the power conversion efficiency of ~8%[5] to ~11%[4].

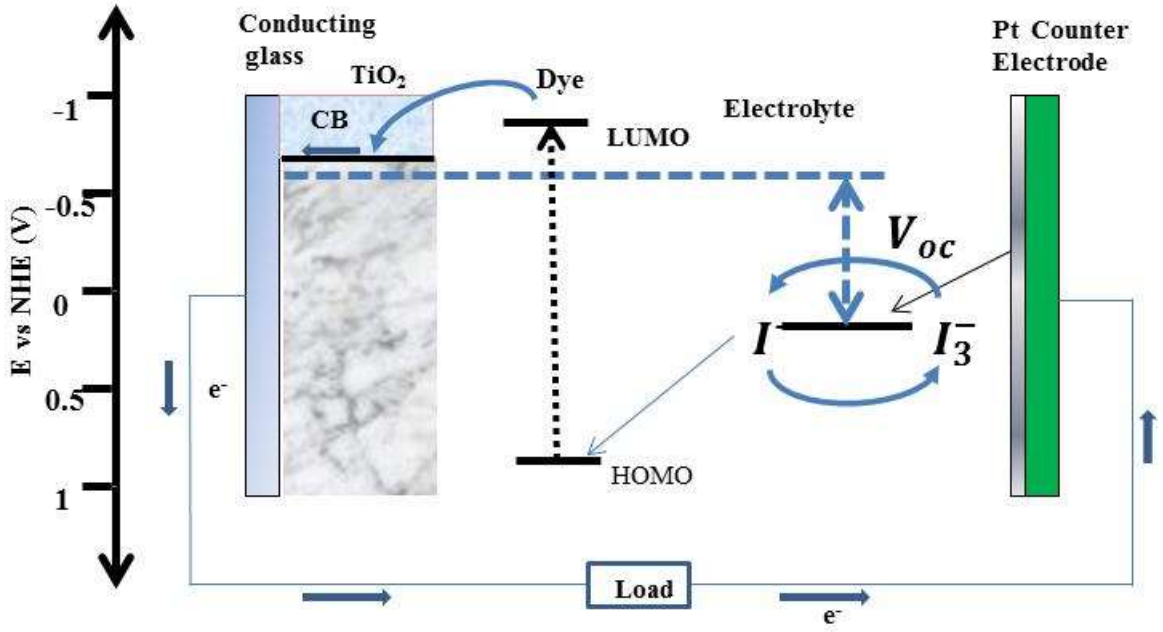

Figure 1.1 Schematic of energy level of components of a DSSC. The cell composed of TiO_2 nanoparticles, dye and a liquid electrolyte containing the iodide/triiodide redox pair. The dashed arrow represents the dye absorbing a photon and promoting an electron from the HOMO level to the LUMO level. The solid arrows represent the path of the electron during cell operation. The maximum possible open circuit voltage, V_{oc}, is the potential between the redox level of the electrolyte and the quasi-Fermi level in the semiconductor under illumination. Energy levels are with respect to vacuum.

1.4 Motivation and objective

Assuming a dye band gap of 2 eV the ultimate theoretical DSSC efficiency, according to the Shockley-Queisser limit, is ~24%[6]. Thus, there is the potential to increase the DSSC efficiency. Replacing the wide band gap semiconductor nanoparticle photoanode in DSSCs with nanowires can potentially improve the solar cell performance due to their direct contact with the electrodes that help to reduce recombination losses and improve short-circuit current on a normalised roughness factor basis[7,8]. The nanowire geometry also allows light absorption and charge separation to be independently optimized thus increasing the overall efficiency[9]. Additionally, nanowires facilitate fabrication of DSSCs directly on low-cost substrates and electrodes such as aluminium foils, conductive glass and stainless steel. These offer the prospective of remarkably low cost fabrication and present attractive features that can facilitate market entry. The ideal diameter and spacing of nanowires arrays is expected to be in the range of 10-20 nm and 20-40 nm respectively, while the desired nanowire lengths are in the range of 50 µm[10]. The lower limit on the interspacing is imposed by the mass transfer limitations on the electrolyte side. This project aims to improve single cell efficiencies by fabricating a nanowire array based photoanode with very high surface area using a bare gold nanoparticle ordered as template with nanoparticle size in the range of 10-20 nm and interspacing ranging from 10 to 30 nm. This should increase the single cell efficiencies to the order of 15-20%, which can make DSSCs attractive for large-scale grid deployment.

2 Literature survey

2.1 Nanowire based dye-sensitized solar cell

The efficiency of nanoparticle DSSC depends on absorption efficiency of solar power, electrolyte used and ease of electron transport in cell. The nanoparticle DSSC absorbs only ~46% of the incident sunlight which limits its efficiency while the electrolyte iodide/triiodide (I^-/I_3^-) is the only known redox couple for which recombination with the electrons in the conduction band of the TiO_2/ZnO is much slower than the electron transport[5,11]. This large ratio of the recombination time constant to the electron transport time constant ensures that almost all electrons injected into the semiconductor are collected[11].

An absorption efficiency beyond ~46% of the incident solar energy can be achieved by increasing the thickness of the nanoparticle layer. This would facilitate more surface area leading to higher dye adsorption followed by improvement in light absorption, and hence an increase in overall power conversion efficiency. However, the efficiency of nanoparticle-based DSSC increases with nanoparticle thickness only up to thicknesses of ~10-20 µm. This is because the electrons transit to the anode by hopping from particle to particle[12]. As thickness increases, the recombination of e^- with another dye molecule or electrolyte also increases[13]. This diffusion length of electrons, L_n, through the nanocrystalline structure are determined to be ~10-20 µm[14]. Thus, when the nanoparticle layer is thicker than ~10-20 µm, more dye is adsorbed, and more light is absorbed, but electrons injected further than L_n away from the anode are less likely to be collected. This implies that electron collection efficiency increases until nanoparticle thickness exceeds L_n while, beyond this length, the electron collection efficiency starts to decrease which causes the overall energy conversion efficiency to saturate.

In order to increase the efficiency of DSSCs by making the photoanode thicker, the electron collection efficiency must also be improved. It can be achieved either by increasing the electron transport and decreasing the recombination rates together or one at a time. Various electrolytes, with faster recombination kinetics but lower redox potential, can be sought which support electron transport as well as add to open circuit voltages. Alternatively, the morphology of photoanode can be changed to nanowire to increase the electron transport rate and/or decrease the electron recombination[7,8]. A schematic of a ZnO nanowire DSSC is shown in Figure 2.1. The mechanism of the DSSC with nanowires as the photoanode is similar to that of the DSSC with nanoparticles. The nanowires ease electron transport by providing a direct electron pathway to the anode. Also, it is not essential for the nanowires to be ordered and vertically oriented; disordered nanowires, each of which is connected to either another nanowire or the anode could also increase electron transport.

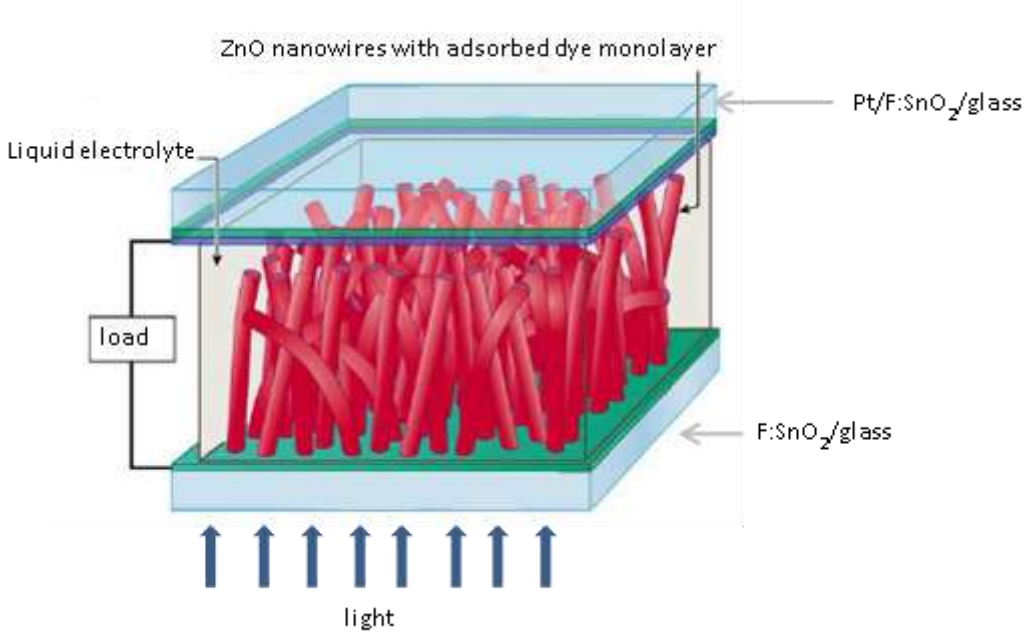

Figure 2.1 Schematic of ZnO nanowire dye sensitized solar cell. [source: Baxter et al][7]

It has been reported that incorporation of nanowires/nanotubes into DSSCs as the photoanode does increase the electron collection efficiency relative to nanoparticles. In particular, the electron transport and recombination rates were found to be increased and equal, respectively, in ZnO nanowires as compared to nanoparticles[15,16]. Nanowire based DSSCs have not attained overall energy conversion efficiencies as high as nanoparticle DSSCs till date. This is attributed to the fact that surface to volume ratio of the nanowire is an order of magnitude lower than that of nanoparticle films[8,17]. This causes less dye adsorption onto the photoanode which leads to lower light absorption and lower overall power conversion efficiencies.

2.2 Properties of ZnO

ZnO is a promising material for nanowire photoanodes in solar cell applications because it is non-toxic, abundant and inexpensive to synthesize[17,18]. It is a natural n-type semiconductor. Besides, it has a wide band gap of 3.3 eV, which enables ZnO to transmit light with wavelengths in the visible and IR range, while providing stability against photocorrosion. ZnO has higher electron mobility than

TiO_2, the most used semiconductor oxide in XSCs, which should favour electron transport. Additionally, the anisotropy inherent in the ZnO wurtzite structure results in ZnO nanowires and nanostructures with a large variety of morphologies to be fabricated with the help of easy and low-cost techniques[18].

2.3 Nanoparticle synthesis

The size and shape of both metal and semiconductor colloidal particles have received much attention in recent years, due to their strong effects on the physical and chemical properties of materials. Therefore, controlled synthesis of nanoparticles plays a pivotal role. A wide variety of techniques has been developed and modified in order to limit the size and shape of the nanoparticles. While synthesizing nanoparticles, factors such as the ability to control mean particle size and its distribution, reaction time, cost and stability of the product have to be considered. Recently, a straightforward and rapid process for the room temperature synthesis of gold nanoparticles using tannic acid has been reported[19]. In this protocol tannic acid, a green reagent, acts as both the reducing agent and stabilising agent. The authors have shown that slow addition of chloroauric acid into tannic acid leads to a colloidal solution of monodisperse gold nanoparticles. The particle size is controlled by a fine balance between rates of reduction and coalescence in the initial period of growth, and the mean size can be tuned from 2-10 nm.

2.4 Template methods for fabricating nanowire arrays

Template methods are introduced to control the position, shape and/or arrangement of nanowires. Our aim is to have a fast and cheap template process with a reliable and independent control of size spacing and diameter. In the past few years, a number of approaches have been used to obtain nanoscale-patterned metal catalyst for successful large-scale fabrication of nanowires arrays. The electron beam lithography (EBL), Nanoimprint lithography (NIL) and soft lithography are among the most cited techniques. However, EBL technique is relatively complicated and expensive and is not adapted for large-scale fabrication. While the EBL technique has been reported for the fabrication of nanowire arrays of InP[20] and ZnO[21], NIL method has also been shown to obtain highly ordered and spatially separated metal dots for subsequent growth of InP nanowire arrays[22]. Soft-lithographic etching route has been used to obtain gold dot patterns[23]. The advantage of their method is that gold dots can be patterned in a large scale with variable geometry and spacing. Homogeneous arranged gold nanodot arrays with the help of gold nanotube membranes (GNM) has also been demonstrated[24]. These fabrication approaches have two main limitations. First, the spacing of the metal dot array is not adjustable in the sub-room range. Second, nanowires have a relatively broad size distribution. These drawbacks may hinder the nanowire arrays from device application consideration. Recently, Muralidharan et al[25] have come up with an easy and scalable process for the formation of large-scale, ordered, 2D arrays of gold nanoparticles upon drop-casting. They have also shown that inter-particle spacing and packing structure in these 2D arrays are controlled by the substrate and the solvent used for drop-casting. These 2D arrays of gold nanoparticles of diameter 7 nm and 20 nm interparticle spacing will be used as template to grow nanowires where gold nanoparticles act as metal catalyst.

2.5 Nanowire synthesis

The growth of nanowires is reported extensively in the literature[26-30]. Here, we focus on two methods most commonly used to fabricate nanowires for solar cells: chemical vapor deposition and electrochemical deposition.

In electrochemical deposition method, nanowires are grown with the help of templates such as porous anodic aluminium oxide (AAO), nano-channel glass, and porous polymer films self-organized from di-block copolymers. The template is attached to the cathode. Subsequently, anode and cathode are brought into contact with the deposition solution. Cations diffuse towards and reduce at the cathode on applying an electric field. Thus, nanowire grows filling the pores of the template. The free-standing nanowires can be obtained by dissolution of the template membrane. The geometry of the pores, which can be tuned by the etching process, determines the dimensions of the nanowires. The most widely used template for electrochemical deposition of NWs is AAO. However, due to the stiffness and hydrophilicity, AAO membrane allows only inhomogeneous pattern transfer.

In chemical vapour deposition (CVD), nanowires are synthesized by reaction of chemical precursor vapours on a substrate placed in the hot zone of a furnace. The substrate may bear metal catalyst nanoparticles and has to tolerate a high temperature. The precursor vapour source can be a gas, liquid or heated solid and is transported to the substrate with an inert carrier gas. Other reactant gases may be supplied along with carrier gas. The substrate is kept at high temperature, where chemical decomposition is favourable. The CVD system has been used to grow ZnO NWs in this report. A number of mechanisms have been cited, in the literature, to explain nanowire growth. Therefore, growth mechanism of ZnO NWs in CVD system will be discussed in detail in section 2.7.

2.6 Growth mechanism of ZnO nanowire

There are numerous methods such as plasma enhanced chemical vapour deposition (PECVD), solution phase growth, inductive deposition, pulsed laser deposition and vapour phase technique which can be used to grow ZnO NWs. The vapour phase deposition is mostly used to grow ZnO NWs and also the main technique in this report. There are many chemical reactions involved during the growth, for example carbothermal reactions. Therefore, the vapour phase technique for ZnO NW synthesis is also called CVD.

2.7 Chemical vapor deposition

Chemical vapor deposition for the growth of ZnO NWs can be explained with the help of three discrete mechanisms described below.

2.7.1 Vapor-Liquid-Solid mechanism (VLS)

The VLS mechanism uses a metal catalyst that forms a liquid eutectic with the desired nanowire material[28,31]. In VLS, an epitaxial nanowire is synthesized via a three-state transformation, starting from vapour phase transport, liquid transformation followed by whisker-like solidification. The vapor phase can be formed through different ways depending on kind of processes and materials used. In our case, Zn vapor is supplied by carbothermal reduction of ZnO powder and, gold nanoparticles act

as catalyst. In the carbothermal reduction, ZnO reacts with graphite or CO (formed in situ) at high temperature ($1000℃$ to form zinc and zinc oxides as follows:

$$ZnO(s) + C(s) \rightarrow Zn(g) + CO(g) \quad (2.1)$$

$$ZnO(s) + CO(g) \rightarrow Zn(g) + CO_2(g) \quad (2.2)$$

$$CO_2(s) + C(s) \rightarrow 2CO(g) \quad (2.3)$$

When Zn vapor transports with carrier gas (N_2 or Ar gas), Zn atoms are deposited onto gold nanoparticles with suitable substrate temperature (T_s). Au has a higher surface energy than Zn and is stable during the heating process, so Zn vapor can easily deposit onto gold nanoparticles. A small amount of deposited Zn atoms diffuses into Au catalyst. The chemical potential of Zn in vapor needs to be higher than that of Zn/Au catalyst for deposition and diffusion of Zn atoms onto or into Au catalyst. The mechanism also insists on condensation of Zn atoms to the point where a deposition occurs to maintain high chemical potential of Zn in vapor. Hence, Zn atoms stay in catalyst rather than in Zn vapor form. Gradually, the Zn concentration increases until the Zn/Au alloy reaches the solid/solid-liquid line of eutectic point and Zn/Au catalyst dissolves into liquid eutectic droplets. When 20% of zinc dissolves in gold, it reduces the melting point of the Zn-Au system to around 800 ˚C whereas the melting point of Au, Zn and ZnO are1064.43 ℃ ,419.58 ℃ and 1975 ℃ respectively[32].The liquid can trap a larger number of Zn atoms. The liquid phase becomes supersaturated with subsequent addition of dissolved species. As the degree of supersaturation overcomes the nucleation barrier, precipitation of Zn starts. The precipitated layers below the Zn-Au drop are oxidized into ZnO by available or supplied oxygen[33] rendering an extremely anisotropic nanowire with well-defined crystal facets and a diameter that is dependent on the size of the particle. Additional flux of Zn vapor leads to further growth of ZnO nanowires. In VLS, a very high growth rate of wire has been found and the gold particle is normally observed to be at tip of ZnO nanowires[33-35]. The VLS process is carried out at higher temperatures (source, substrate) resulting in a faster evaporation of the source causing a faster supply of Zn vapor into the gold nanoparticles. This further intensifies the oversaturation and hence feeding of the growing nanowires by the Zn-Au droplet.

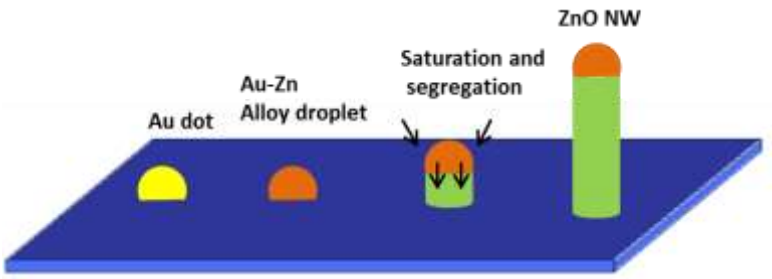

Figure 2.2 Schematic illustration of ZnO nanowire growth by VLS mechanism, from gold dot, Zn/Au liquid phase, saturation and growth.

The experimental conditions (source temperature, substrate temperature and deposition temperature) favouring well aligned nanowires of diameters above 50 nm by VLS technique have been reported in literatures as shown in **Figure 2.3** and **Figure 2.4**. The source temperature and the substrate temperature should be kept in the range of $900 - 950$ ℃ and $800 - 850$ ℃ respectively

while pressure can vary from 3-10 mbar. Song et al has correlated the deposition pressure to partial pressure of oxygen in the chamber as shown in **Figure 2.5**. In the phase diagram, dark red represents the best growth condition. It corresponds to a pressure range between 7-30 mbar where a perfect alignment and ZnO nanorods with a high density and uniform length and thickness can be achieved.

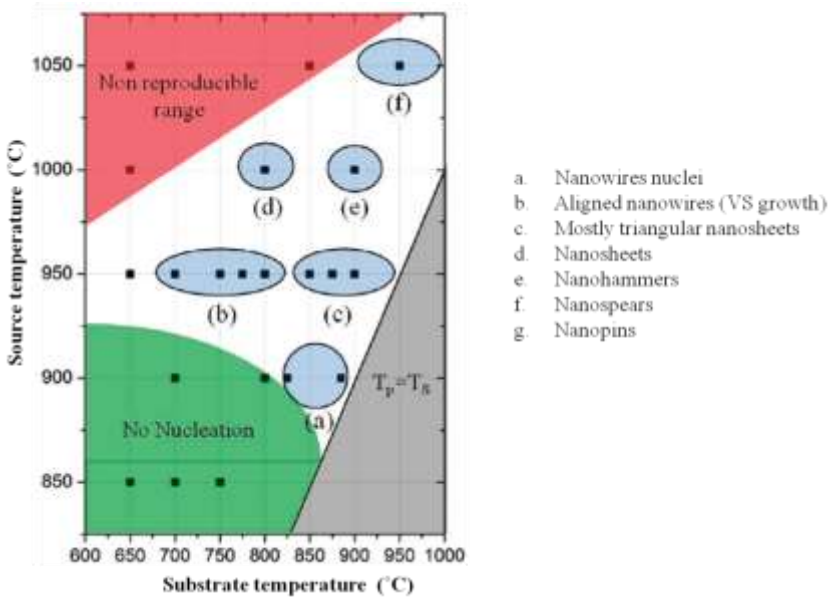

Figure 2.3 Shape diagram of ZnO nanostructures formed including (a) nanowires nuclei, (b) nanowires, (c) mostly triangular nanosheets, (d) nanohammers, (e) nanospears, and (f) nanopinsas a function of at source temperature (T_p) and substrate temperature (T_s). [source : Wonchoosuk et al][36]

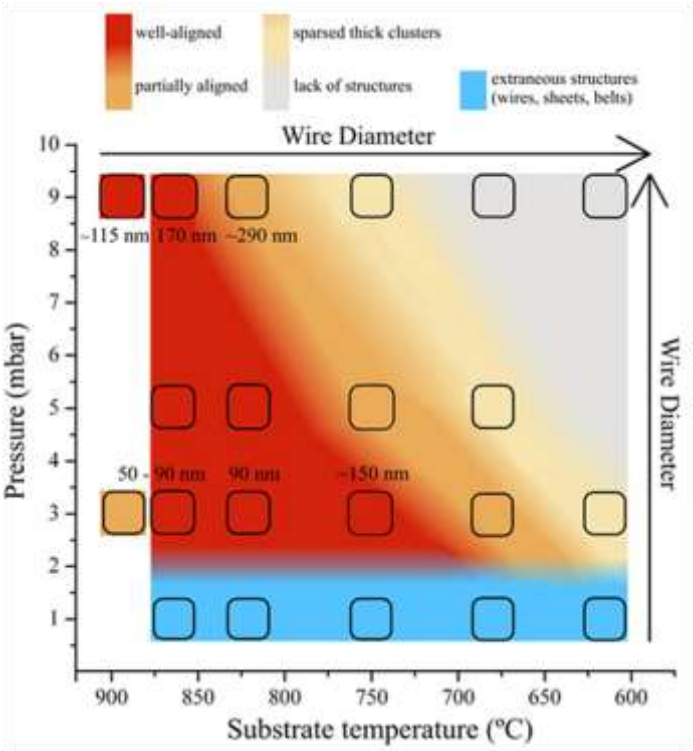

Figure 2.4 Phase diagram of pressure and temperature showing growth zones of various ZnO nanostructures.[source : Dalal et al][37]

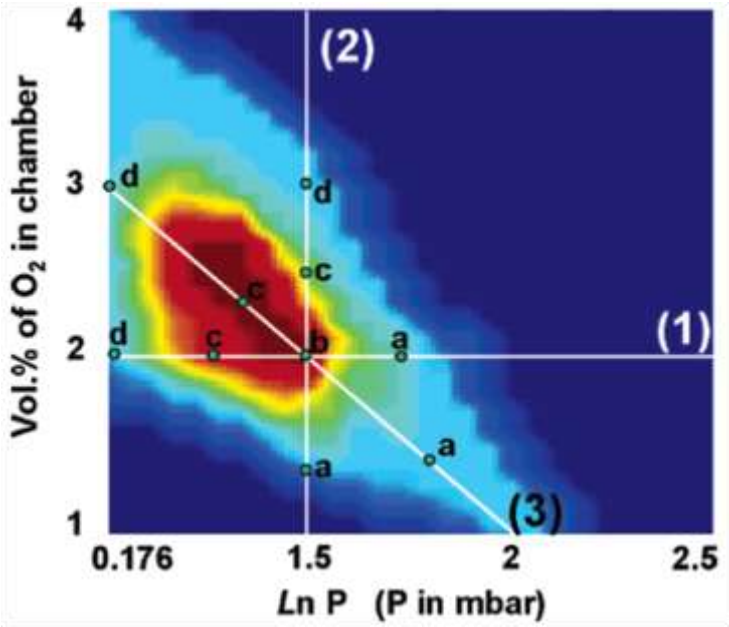

Figure 2.5 Phase diagram that correlates oxygen volume percent in the growth chamber and the growth chamber pressure (plotted in logarithm and P is in unit of mbar) for growing aligned nanorods. The synthesis line (1) is the line with constant oxygen volume percent; line (2) is the line with constant pressure; line (3) is the line with linearly varying oxygen volume percentage and system pressure.[source : Song et al][38]

2.7.2 Vapor solid mechanism (VS)

The vapor solid mechanism lacks liquid phase transformation. In this case, gold acts as surface defect or selective site for Zn vapor deposition. Like VLS technique, zinc

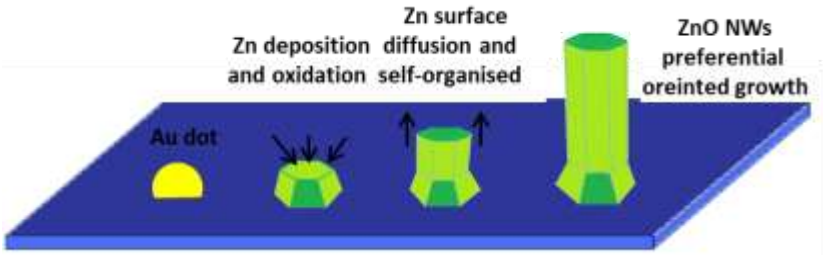

Figure 2.6 Schematic illustration of ZnO nanowire growth by VS mechanism, from gold dot, surface diffusion, saturation and growth

vapor transports with carrier gas and deposits onto gold nanoparticle. After deposition, Zn atom is immediately oxidized by abundant O_2 without having the possibility to diffuse into the gold dot[39]. Hence, it is always pronounced mechanism in a high oxidation environment. When vapor transforms to solid phase, the chemical potential of Zn in vapor must be greater than in a ZnO crystal. The supersaturation and epitaxial growth of ZnO nanowires occurs at the gold dot without the fast diffusion and the segregation from an gold nanoparticle. As a result, a kind of pyramidal nuclei overgrows very fast from the selective site, and Au nanoparticles are buried underneath nanowires[39]. Afterwards, ZnO nanowires grow due to surface diffusion of incoming Zn vapor. However, deposition of Zn vapor occurs preferentially at metal nanoparticle, and Zn atoms move to a single preferential orientation due to surface diffusion. It implies that deposition of Zn vapor in the VS mechanism is limited to the catalyst and ZnO surface whereas deposition is more pronounced due to adsorption onto eutectic liquid in the VLS mechanism. Therefore, the VS growth is 10-100 times slower than the VLS growth[40]. The gold dot is absent at the tip of nanowire and characteristic hexagonal structure of ZnO can be observed.

2.7.3 Vapor-solid-solid mechanism (VSS)

The VSS mechanism is similar to VLS growth. It occurs at low temperature (below 500-400 ℃). In this case, Zn atoms deposit on gold catalyst by vapor phase transport, and diffuse to form Zn/Au alloy. However, the catalyst remains solid instead of forming a eutectic liquid due to low substrate temperature. The Zn concentration in Zn/Au solid alloy keeps increasing till the saturation limit. At this point, Zn precipitates on catalyst and oxidized resulting in epitaxial ZnO nanowires. Unlike the VLS mechanism, gold cannot be observed on the tip of grown nanowire.

3 ZnO nanowire growth

Synthesis of ZnO nanowires has been studied in following steps. In the beginning, self-assembly of Au nanoparticle arrays is obtained by following work of Muralidharan et al[25] on Si substrate having thick layer of SiO_2. The SiO_2 layer is deposited by annealing Si wafer at 500 ℃ for 45 min in presence of O_2. The substrate is subjected to high temperature to check thermal stability of nanoparticle arrays. Finally, the substrate is kept in two zone tubular furnace to grow nanowires by vapor phase deposition.

3.1 Fabrication of gold nanoparticle array

Thiol terminated polystyrene (PSSH, 20000 MW) have been shown to give hexagonal pattern of gold nanoparticles array, but available PSSH were shipped before 18 months. The manufacturer *polymer source Inc* claims,

"We have observed that these polymers are very sensitive to air and light which form disulfide linkage (in 3-4 weeks time) even after storage under vacuum at low temperature. We check each lot before shipment and convert disulfide fraction back to free thiol if any change observed. The shelf-life of such polymers at low temperature is found to be 3-5 weeks after shipment."

Source :http://www.polymersource.com/product.php?ID=696

Nanoparticles capped with disulfide linked polymer give non-uniform array and multi-layer array. Due to the high cost of polystyrene thiol, devising ways to obtain monolayer array of gold nanoparticles by using available thiol- terminated polystyrene becomes significant. A series of experiments were carried to reduce internal disulfide linkage to functionalized polymer thiol.

3.2 Reduction of disulphide linkage

A variety of reagents for reduction of internal disulfide bond has been described in the literature, due to its applications in protein chemistry and biochemistry[41,42]. Dithiothreitol (2,3-dihydroxy-1,4-butanethiol, DTT) is selected for the purpose of this study because of several reasons. First, DTT is an unusually strong reducing agent which can be explained by the stability of the six-membered cyclic sulfide formed after the oxidation of this dithiol. It reduces a typical disulfide bond by two sequential thiol-disulfide exchange reactions. The intermediate mixed-disulfide state is unstable because the second thiol of DTT has a high propensity to close the ring leaving behind a reduced disulfide bond. Its principal advantage is that effectively no mixed-disulfide species are generated, in contrast to other agents such as glutathione.

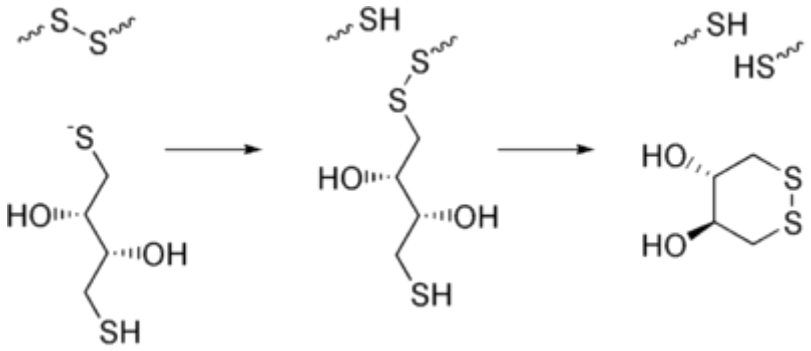

Figure 3.1 Reduction of a typical Reduction of a typical disulfide bond by DTT via two sequential thiol-disulfide exchange reactions.

In addition, DTT is highly soluble in a range of solvents including those that dissolve polystyrene such as THF and DMF.

3.3 Recovery of thiol-terminated polystyrene

In all the following experiments, gold nanoparticles of 7 nm diameter used were prepared by Sivaraman's protocol that uses tannic acid as both reducing and stabilizing agent[19]. They were capped with treated thiol terminated polystyrene as reported by Muralidharan et al[25]. Typically, 0.4 mL of 1% by weight of sodium citrate is added to 10 mL of tannic acid capped gold nanoparticle solution and boiled with 3 mL of hydrogen peroxide. After cooling, 5 mL of this solution is added to 1.5 mL of 0.1% by weight of processed polystyrene thiol.

1. An experiment was carried out following method of Muralidharan et al[25] using aged PSSH. Briefly, 1.5 mL of 0.1% by weight of PSSH was added to 5 mL of tannic acid capped gold nanoparticle solution along with 5 mL acetone. The resulting solution was centrifuged at 3500 rpm after 8 h. The precipitate was

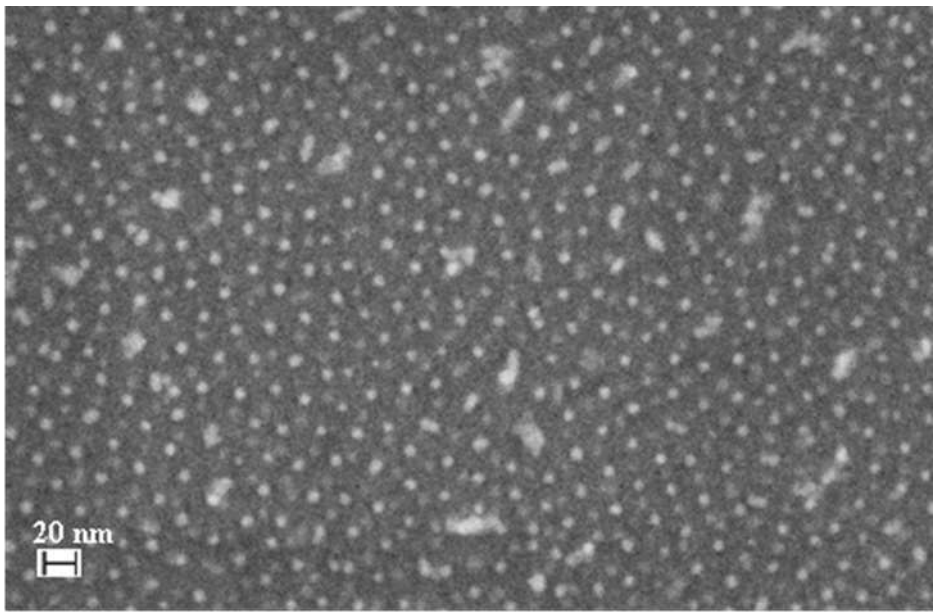

Figure 3.2 FESEM image of nanoparticle array with the use of aged thiol terminated polystyrene. The image shows nanoparticles of higher contrast above the layer of nanoparticles of lower contrast. The capping of gold nanoparticles with functionalized thiol as well as disulfide linkage in polymer causes arrangement in multilayers.

washed with acetone twice and centrifuged. The precipitate was dried, and dissolved in toluene prior to drop-casting on a silicon wafer. The SEM image shown in **Figure 3.2** indicates that the nanoparticles with higher contrast are arranged in a layer above the layer of nanoparticles with lower contrast. However, the gold nanoparticles capped with PSSH arrange in hexagonal pattern in monolayer[25]. The multi-layer arrangement of nanoparticles implied that nanoparticles had been capped with internal disulfide linkage in degraded polymer, in addition to thiol terminated polystyrene. The washing, with acetone alone, was not sufficient to remove degraded polymer.

2. Since the presence of disulfide linkage in polymer end up with multilayer nanoparticle array, above experiment was repeated with some modification in centrifugation step. 5 µL of chloroform was added to the precipitate followed by 5 mL of acetone. The solution was centrifuged at 3500 rpm and again washed with acetone. The precipitate so obtained was allowed to dry and then

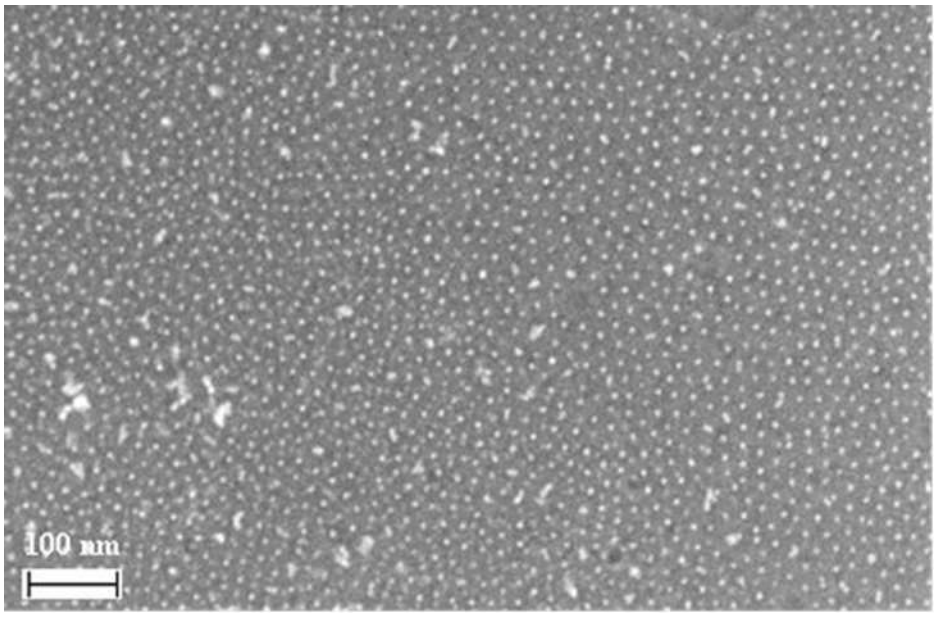

Figure 3.3 FESEM image of nanoparticle array with the use of available thiol terminated polystyrene after centrifuging at 3500 rpm followed by 15000 rpm. During centrifugation, 5 µL chloroform was added along with acetone to remove disulfide linkage. The addition of chloroform generated a monolayer at several spots along with multilayer of nanoparticle arrays.

drop-cast on silicon dioxide wafer after dissolving in toluene. Chloroform is used to dissolve disulfide, but it also results in loss of nanoparticles with supernatant. The

supernatant was centrifuged to minimize the loss of particle at 15000 rpm. The SEM image of nanoparticle array after centrifuging at 3500 rpm followed by 15000 rpm is shown in **Figure 3.3**. This modification was able to generate monolayer at several spots along with multilayer of nanoparticle array. However, loss of particle during centrifugation leads to irreproducibility of results.

3. It has been shown that disulfide linkage can be reduced to thiol group by adding excess moles of DTT in deoxygenated solvent like THF or DMF under nitrogen[42]. In a typical procedure, the polymer with internal disulfide linkage ($(6.4 - 7.0) \times 10^{-6}$mol) was dissolved in 10 mL of deoxygenated DMF, containing DTT (3.25×10^{-4}mol).The mixture was stirred under nitrogen at 60°C for 24 h. Methanol (deoxygenated by purgingwith nitrogen; 2 mL) was

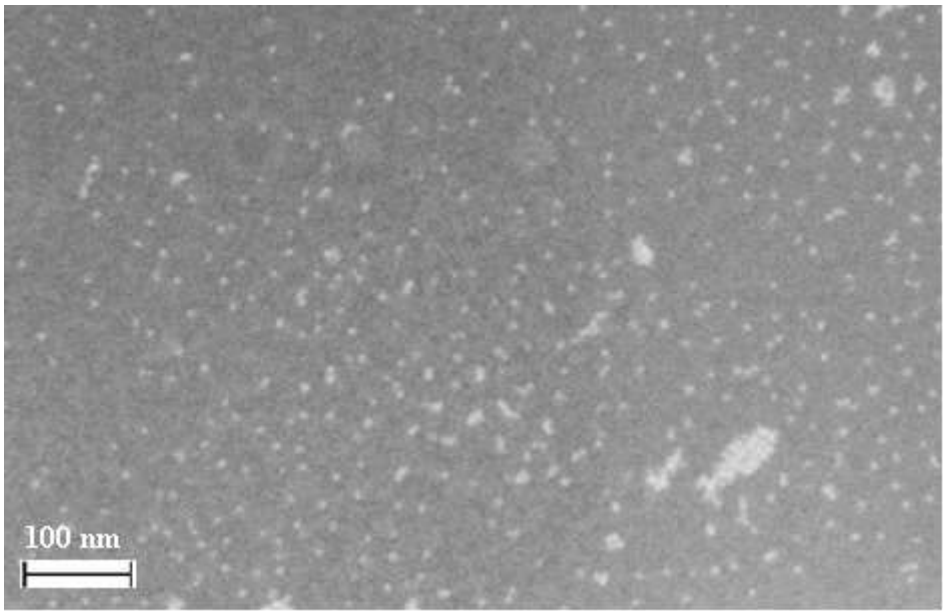

Figure 3.4 FESEM image of nanoparticle array with the treated thiol terminated polystyrene. Thiol terminated polystyrene was reacted with excess DTT under nitrogen at 60˚C for 24 h. The random arrangement of nanoparticles suggests that the recovery of free PSSH adding excess DTT is minimal.

then added, and the mixture was stirred at 50˚C for another 3 h. The precipitated polymer was filtered off and washed on the filter with deoxygenated methanol. It was expected that the collected polymer contained only small amount of dimer and no higher oligomers. The precipitate was allowed to dry overnight and used further to cap gold nanoparticles. After drop-casting on silicon dioxide wafer, only random distribution of nanoparticles was observed as shown in **Figure 3.4**. This suggests that the recovery of free PSSH by this method is minimal.

4. In the previous experiment, excess moles of DTT were used to reduce disulfide bond and methanol was added to dissolve remaining DTT after reaction. It is difficult to estimate the extent of oxidation of PSSH and determining the exact level of washing required. So, an experiment was carried using 30% DTT by molar ratio to that of PSSH. These were allowed to react for 6 h in three different centrifuges. Then, 5 mL of tannic acid capped

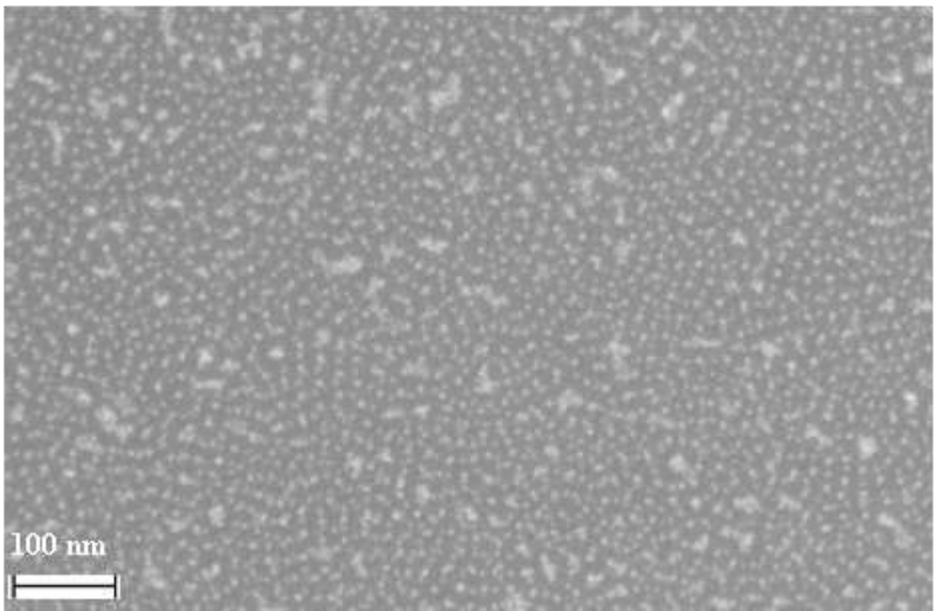

Figure 3.5 FESEM image of nanoparticle array with the treated thiol terminated polystyrene. Thiol terminated polystyrene was reacted with 30% DTT and allowed to cap gold nanoparticle for 45 min (Sample **A**). It shows arrangement of nanoparticles in multi-layer only.

gold nanoparticle solution was added to each of them and left for 45 min, 2 h and 6 h respectively. Precipitate was collected after acetone wash and centrifugation, and allowed to dry. The precipitate was drop-cast on silicon dioxide wafers, and the substrates were observed under SEM. Sample **A** (corresponding to 45 min) has only multilayer of nanoparticle arrays (**Figure 3.5**). Sample **B** has mixed regions of monolayer as well as multilayer of arrays (**Figure 3.6**) while Sample **C** has relatively large patches of monolayer in comparison with multilayers (**Figure 3.7** and **Figure 3.8**). Increase in the area of monolayer of nanoparticle arrays suggests that cleavage of disulfide bond by DTT improves with time to a great extent. The appearance of multilayers is attributed to remaining disulfide linkage. Sample **B** also shows nanoparticles with very small interparticle spacing, which may be due to capping of gold nanoparticles by DTT.

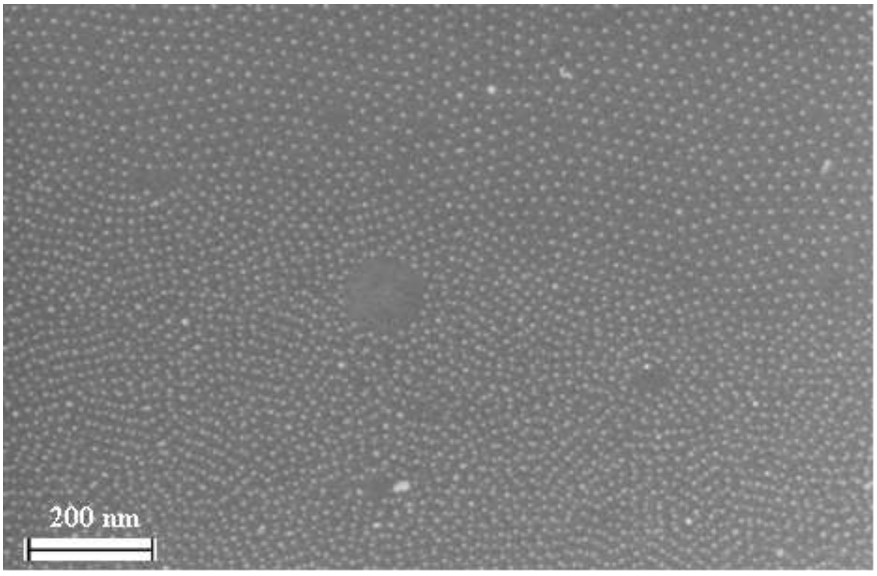

Figure 3.6 FESEM image of nanoparticle array with the treated thiol terminated polystyrene. Thiol terminated polystyrene was reacted with 30% DTT and allowed to cap gold nanoparticle for 2h (Sample **B**).The image shows mixed regions of monolayer and multilayer of arrays. It also indicates nanoparticles with very small interparticle spacing, which may be due to capping of gold nanoparticles by DTT.

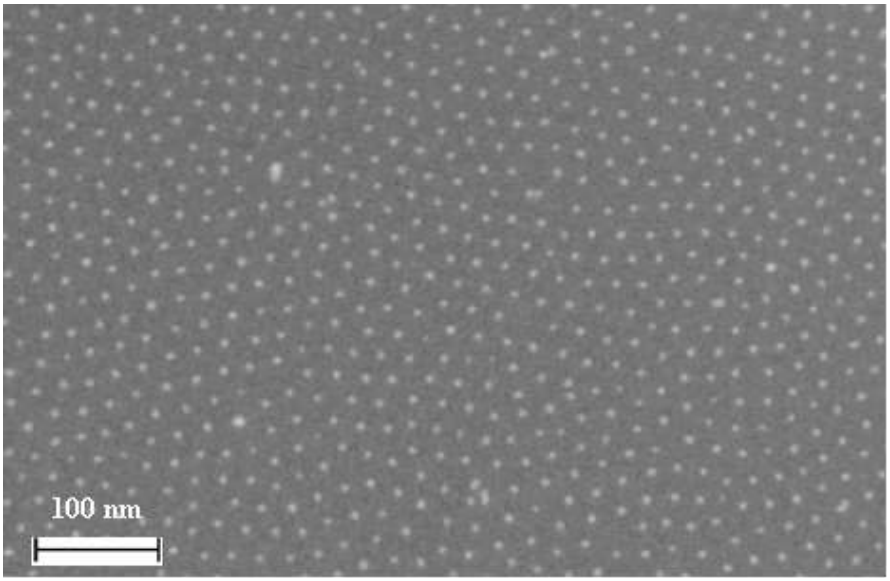

Figure 3.7 FESEM image of nanoparticle array with the treated thiol terminated polystyrene. Thiol terminated polystyrene was reacted with 30% DTT and allowed to cap gold nanoparticle for 6 h (Sample **C)**. It shows monolayer of nanoparticle arrays in hexagonal pattern. Such patterns of monolayer were observed on relatively large patches of substrate in comparison with multilayers.

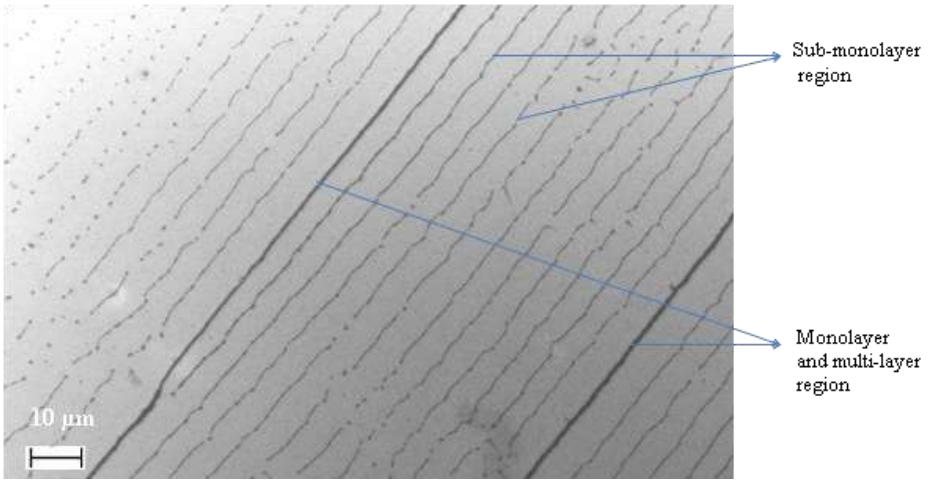

Figure 3.8 Large scale FESEM image of nanoparticle array with the treated thiol terminated polystyrene. Thiol terminated polystyrene was reacted with 30% DTT and allowed to cap gold nanoparticle for 6 h (Sample **C)**. It shows pattern of monolayer of nanoparticle arrays across sample. The patterns of monolayer were observed on relatively large patches of substrate in comparison with multilayers.

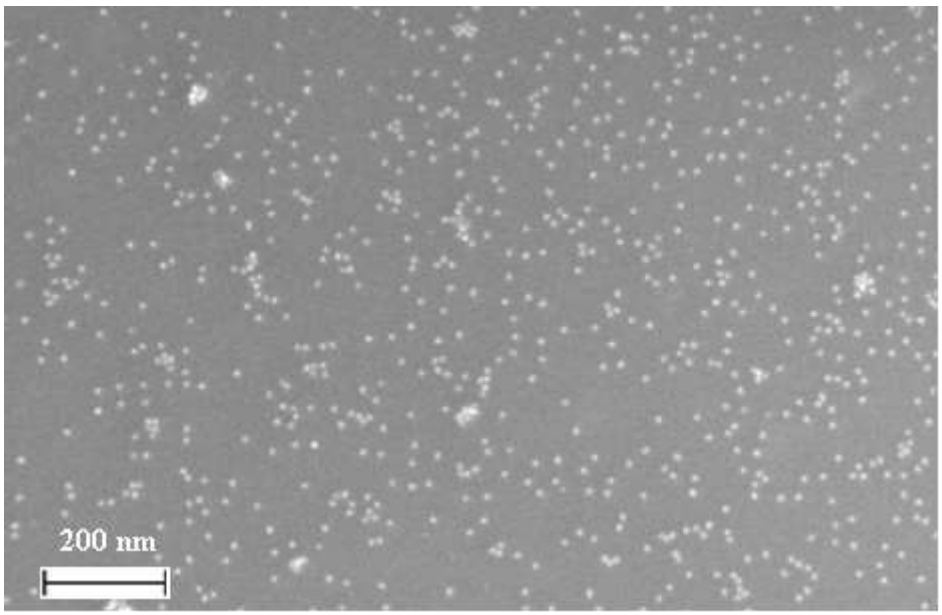

Figure 3.9 FESEM image of nanoparticle array with the treated thiol terminated polystyrene. Thiol terminated polystyrene was reacted with 30% DTT and passed through desalting column. The monolayer of nanoparticle shows that disulfide linkage has been reduced to thiol-functionalized PSSH. Lower interparticle spacing at various places indicates the presence of DTT gold nanoparticles.

5. This experiment was done in an attempt to remove unreacted DTT, if any, when 30% DTT by molar ratio to that of PSSH and allowed to react for 6 h. In the first case, 5 mL of tannic acid capped gold nanoparticle solution was mixed to reacting solution of PSSH and DTT, and allowed to cap nanoparticle for 6 h. Since methanol is a strong

solvent for DTT, so 2 mL of methanol was added. The solution was centrifuged after 2 h, but the particles remain suspended in solution, and the sample was discarded. In the second method, mixture of PSSH and DTT was allowed to pass through a desalting column and collected solution was processed to cap gold nanoparticles for 6 h. The precipitate obtained after centrifugation was used for drop casting and observed under SEM. It shows random arrangement of nanoparticles across the sample with minimal presence of multilayer as shown in **Figure 3.9**. The arrangement of nanoparticles with very small interparticle spacing indicates the presence of DTT capped gold nanoparticles. This implies that DTT has not been removed completely by desalting column.

6. While last experiment was focused on removal of DTT, this experiment was centred towards treatment of remaining disulfide linkage by increasing molar ratio of DTT. Now 40% DTT by mole was added to PSSH and left for 24 h. Thereafter gold nanoparticles were mixed to it and allowed to cap for 30 h. The solution was centrifuged at 3500 rpm. 10 µL of chloroform was added to precipitate along with 5 mL of acetone and centrifuged again. At last, the precipitate was allowed to dry and drop-cast after dissolving in toluene. The SEM image (**Figure 3.10** and **Figure 3.11**) of sample shows hexagonal pattern of monolayer of nanoparticle array in many areas of substrate. This experiment was successfully repeated to check the reproducibility of array formation. Hence array so obtained lets us move towards the next step of nanowire growth.

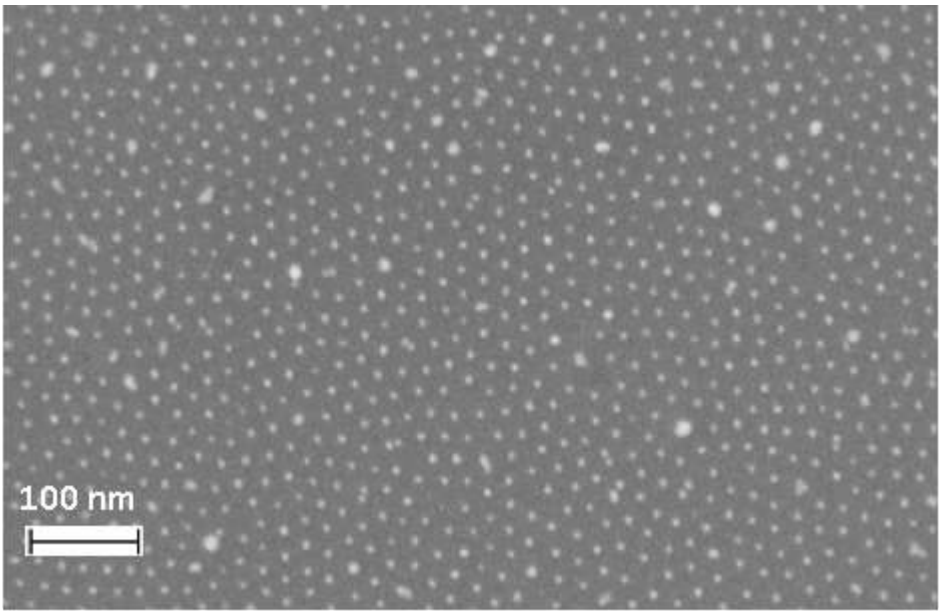

Figure 3.10 FESEM image of nanoparticle array with the treated thiol terminated polystyrene. Thiol terminated polystyrene was reacted with 40% DTT for 24 h and allowed to cap gold nanoparticle for 30 h. 10 µL chloroform was also added during centrifugation. The image shows monolayer of nanoparticles arranged in hexagonal pattern. Such patterns of monolayer were observed on most parts of the substrate as shown in **Figure 3.11**.

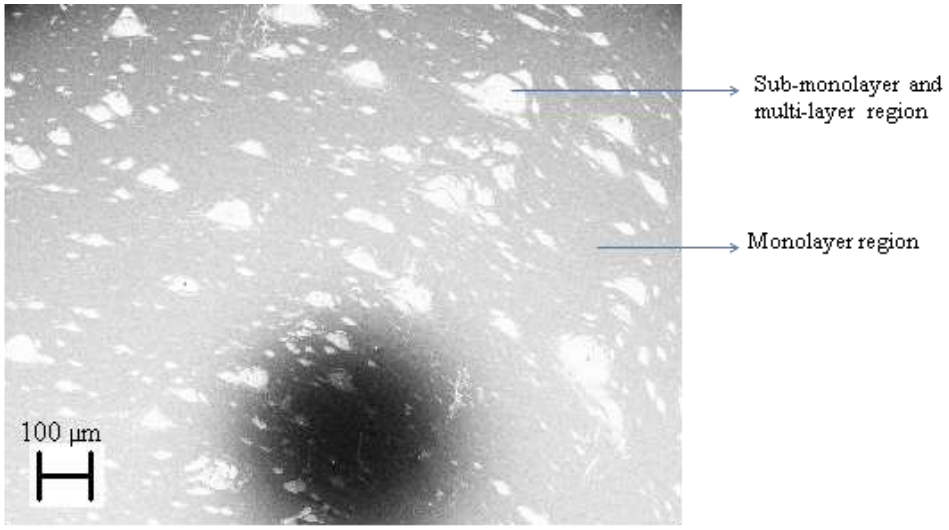

Figure 3.11 Large scale FESEM image of nanoparticle array with the treated thiol terminated polystyrene. Thiol terminated polystyrene was reacted with 40% DTT for 24 h and allowed to cap gold nanoparticle for 30 h. 10 µL chloroform was also added during centrifugation. The image shows that main area is covered by monolayer of nanoparticle arrays.

3.4 Thermal stability of nanoparticle arrays

Thermal stability of nanoparticle array was ascertained in this experiment as substrate had to be kept at 550-600˚C. Nanoparticle array, obtained on Si Wafer coated with

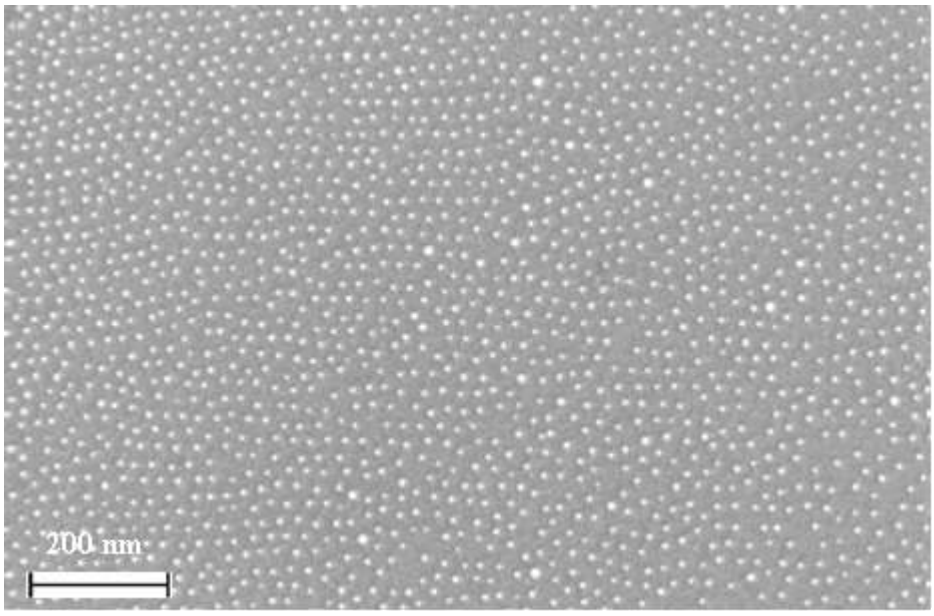

Figure 3.12 FESEM image of nanoparticle array with the treated thiol terminated polystyrene. Si wafer was coated with 1 µm thick SiO_2, drop casted with nanoparticle array, treated with O_2 plasma for 8 min and heated in temperature regime of 550-600˚C for 45 min at 5 mbar with Ar flow at 200 sccm. It shows nanoparticles have not fused while heating.

1 µm thick SiO_2, was subjected to O_2plasma for 8 min to remove polystyrene thiol. The substrate was kept in the regime of 550-600˚C, and heated for 45 min at 5 mbar with Ar flow at 200 sccm. The SEM image of heated substrate (**Figure 3.12**) shows that nanoparticle array is stable at temperature ~600 ℃. The thermally stable Au nanoparticle array was used as catalyst to study the growth of ZnO nanowire by the VLS technique in a high temperature tubular two zone furnace.

3.5 Two zone furnace system

The picture of the two zone furnace system used to grow ZnO nanowires by vapor phase deposition is shown in **Figure 3.13**.The configuration of this system is shown

Figure 3.13 High temperature tubular two zone furnace

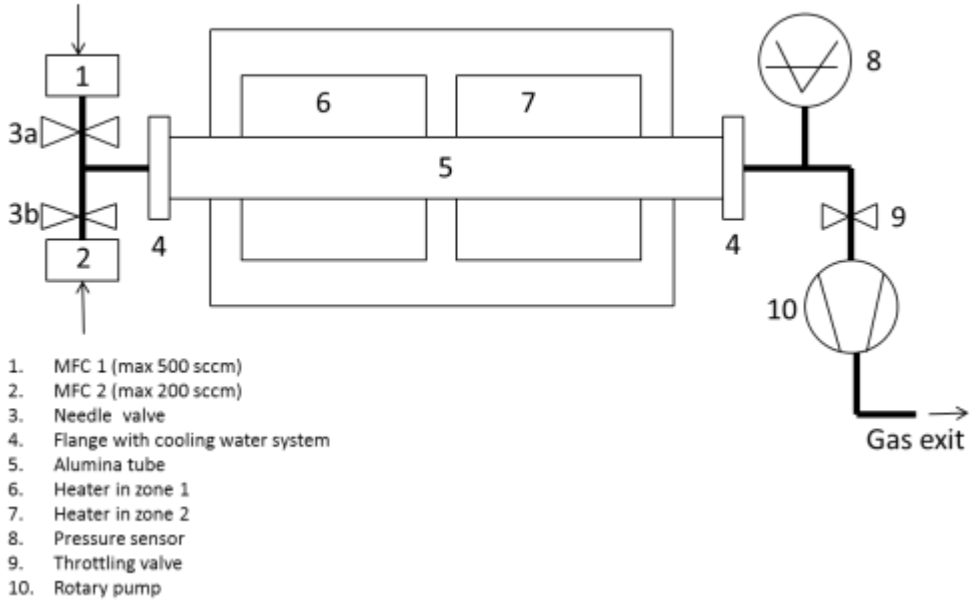

Figure 3.14 Schematic of the two zone system setup for ZnO nanowires.

in **Figure 3.14**. The system setup comprises of the gas input units (1, 2, 3), cooling units (4), growth units (5, 6, 7) and gas output units (8, 9, 10). The input gas is pure Ar or N_2 (99.99%) running through a mass flow controller (ball type) No.1 followed by a needle valve No. 3. Another input unit is provided to flow O_2through mass flow controller No. 2. The mass flow controller No.1 & 2 are rough controller with maximum flow rate of 500 sccm and 200 sccm respectively. In our case, we are investigating the growth of ZnO without flowing reactive O_2 as Ar/N_2 contains 0.002% O_2 as impurity. The needle valve can be used as final gate between the input gas and the rest of the growth system. The next is an alumina tube (No. 5, 7 cm inner diameter and 100 cm length) placed inside the two zone furnace (No. 6 & 7). ZnO NWs can be grown in the alumina tube. However, only one zone (No. 6) is the only presented system to grow ZnO NWs in this thesis. The output unit composes a pressure sensor (Hind High Vacuum), and a manual throttling valve. The output gas has been removed by a 2-stage rotary vane pump (adixen, 2010C1), with a pump rate of 10 m^3/h.

3.5.1 The standard experimental procedure

The experimental procedure to grow ZnO NWs can be explained as the following. First of all, ZnO powder (99.0% purity, S.D. Fine Chemical Ltd.) and graphite powder (99.5% purity, S.D. Fine Chemical Ltd.) are mixed with a 1:1 weight ratio and is used as the source. The source powder is kept at 950 ℃ in zone 1. Silicon wafer, coated with thick layer of SiO_2 and bearing Au nanoparticle arrays, is used as a substrate. The substrate is placed in downstream with respect to the source at 950 ℃. The schematic of the experiment setup is shown in **Figure 3.15**. The system is pumped down to a pressure of 2×10^{-2} mbar to remove air, impurity gases and residual O_2.The needle valve No. 3a is opened and pure Ar/N_2 is supplied at 100 sccm for 10 min into the system to dilute and purge away the remaining O_2. After purging steps, the furnace is heated up to 1000 ℃ and gas is kept flowing while ramping. The furnace is maintained at 1000 ℃ for different times to study the growth of ZnO nanowires. Thereafter, the heater is switched off and furnace is allowed to cool under several

pressure conditions under Ar/N_2 gas flow at 100 sccm. The furnace takes approximately 7 hrs. to cool down to room temperature.

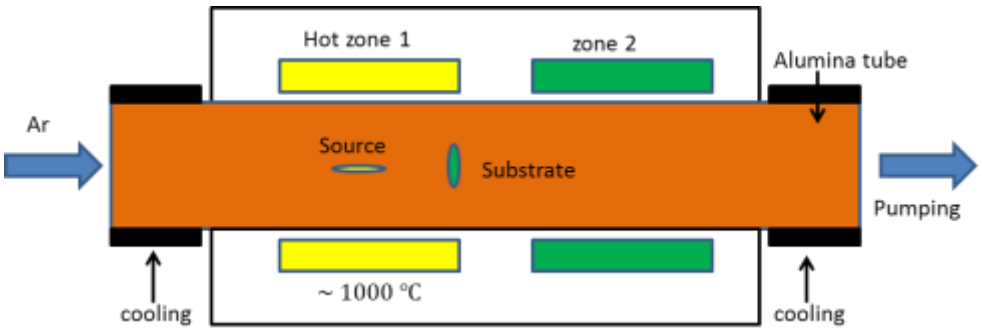

Figure 3.15 The schematic of two zone system during the ZnO nanowires experiment. The source contains ZnO and graphite powder in 1:1 ratio by weight. The substrate is Si wafer having Au nanoparticle on thick SiO_2 layer.

3.5.2 The temperature profile

The exact temperature profile during experiment in the tubular furnace is ard to identify due to its primitive setup. Therefore, the temperature profile is measured by using a thermocouple at a standard growth temperature of 950 ℃. It enables us to keep source and substrate at a specified temperature regime during nanowire growth. The temperature profile is shown in **Figure 3.16** and **Figure 3.18** for a double as well as a typical tubular furnace system respectively. The diameter and length of inner alumina tube are 1.5 cm and 23 cm respectively and is kept in zone 1 as shown in Figure 3.17.When the set temperature is 1160 ℃, temperature at the closed end and open end of small tube is 1000 ℃ and 400 ℃ respectively.Temperature does not vary much with change in flow of Ar gas from 25 sccm to 225 sccm and the profile is found almost similar to that under N_2 gas. In single tubular furnace, the source and substrate have been kept at 950 ℃ and 850 ℃ respectively. The gradient is very strong and these positions are 3 cm apart.

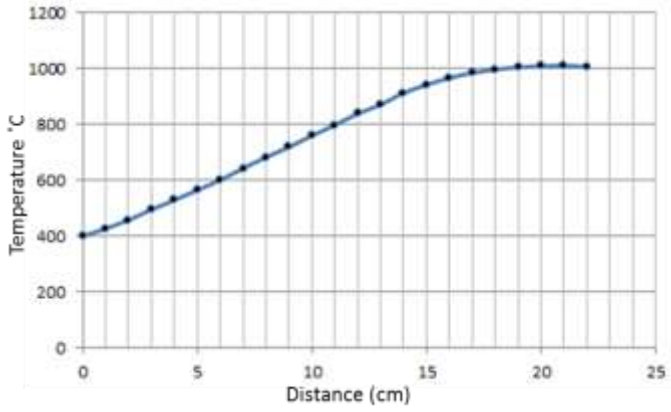

Figure 3.16 Plot showing temperature variation along small tube inside furnace. Temperatures were measured in zone 1 and pressure was maintained at 5 mbar with 200 sccm Ar flow. Set temperature of heater was 1160 ℃.

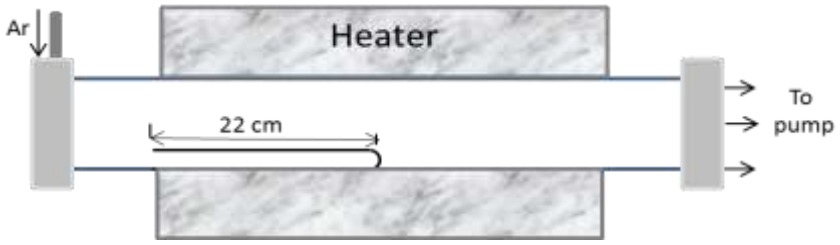

Figure 3.17 Schematic of double tube furnace system

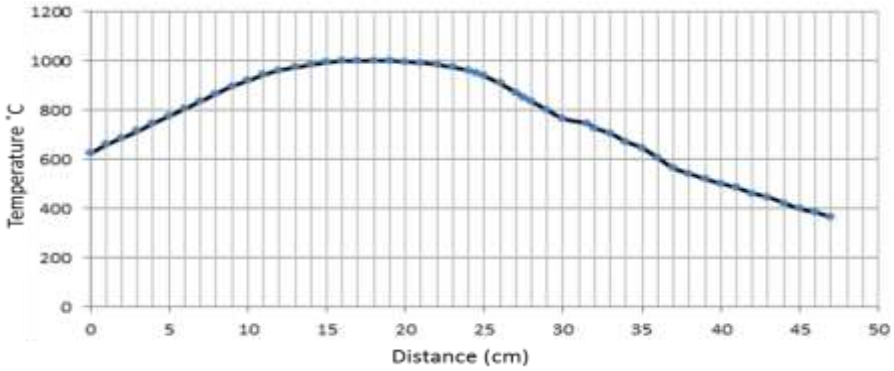

Figure 3.18 Plot showing temperature profile inside horizontal tubular furnace. Temperatures were measured in zone 1 and pressure was maintained at 0.02mbar with 100 sccm N_2 gas flow. The set temperature of heater was 1160 ℃.

3.5.3 Baking of the furnace

The furnace needs baking to prevent effect of previous experiments on the subsequent experiment. The standard experimental procedure was followed to study the

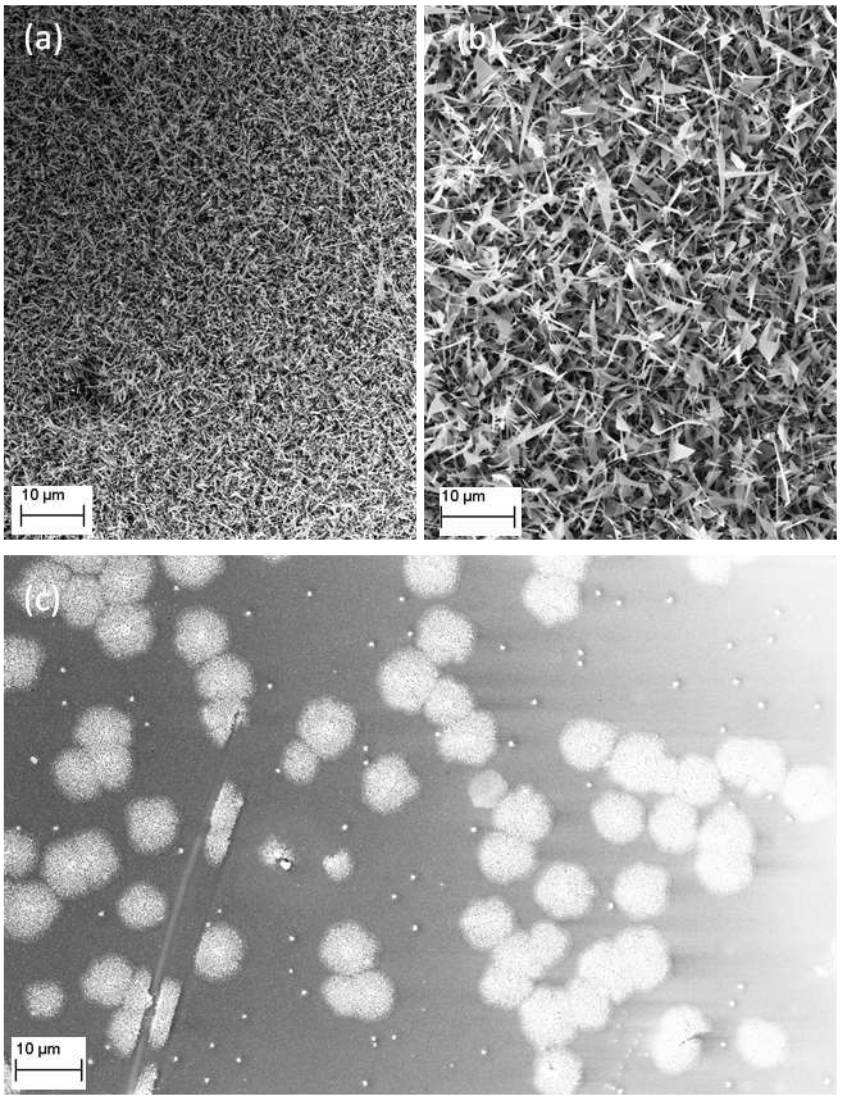

Figure 3.19 The comparison of between SEM images of ZnO nanowires by VLS technique performed (a) & (b) after baking and (b) without baking of the furnace . The study was done under identical experimental conditions. Weight of ZnO - 0.25 g. Weight of graphite – 0.25 g. Source temperature ~ 950 ℃ , subsrate temperature ~ 850 ℃, N_2 flow rate – 200 sccm chamber pressure – 19 mbar. The image indicates uncontrolled growth of nanostructures in (a) and (b) everywhere whereas random in (c).

reproducibility of results. The furnace was ramp up to 1000 ℃ at 0.88 mbar with continuous supply of N_2 at 100 sccm. The source and the substrate were kept at 950 ℃ and 850 ℃ respectively for 15 min at 19 mbar. Then, the furnace was shut down and the substrate was allowed to cool under N_2 flow at 19 mbar. The growth of nanostructures was quite different when the experiment was carried without baking as shown in **Figure 3.19**. The nanostructures were observed across samples in experiments performed after baking of the furnace while random when carried without baking. It implies contamination of furnace tube due to past experiment. The furnace is baked at 850 − 1000 ℃ for 2 hours and allowed to cool under vacuum. The set temperature of zone 1 and zone 2

are 1160 ℃ and 850℃ respectively. Hence, the baking was found to be crucial to minimize the contamination on the walls of tube and was performed before each experiment.

4 Results and discussion

4.1 ZnO nanowire growth in double-tube furnace

In the beginning, the synthesis of nanowires was performed in the horizontal double-tube system. The source material, powdered mixture of ZnO and graphite powder (weight ratio 1:1), was placed at the closed end of the small alumina tube and the substrate was located at the open end of the small tube in the temperature zone of550-600˚C. The relevant distances are marked in **Figure 4.1**. The smaller tube was then inserted into the large tube. The closed end of the small tube was positioned at the center of the larger one. The system was pumped down to a base pressure of 3.5 mbar, and then argon was passed through the tube at a constant flow rate of 200 sccm. The temperature of the furnace was ramped to 1160˚C, kept at that temperature for 45 min, and then cooled down to room temperature naturally. During the whole experiment, the argon flow rate was kept at 200 sccm and pressure 3.5 mbar.

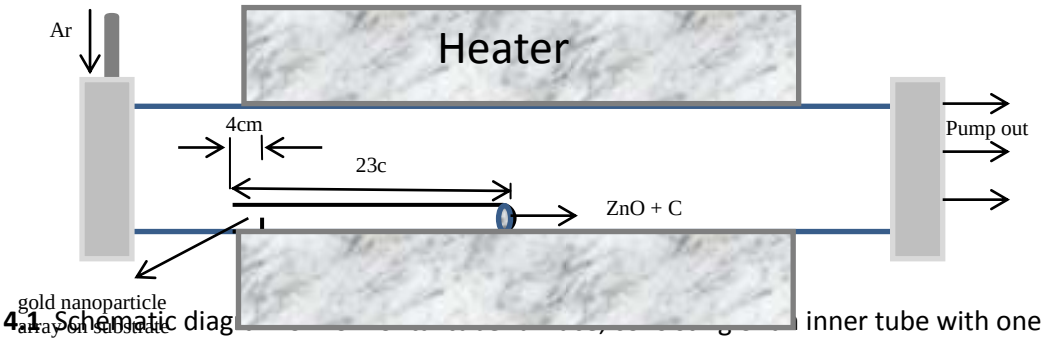

Figure 4.1 Schematic diag inner tube with one closed end, used for nanowire synthesis.

Gray-colored products were found on the silicon substrate. The morphologies and microstructures of the as-synthesized products were observed by SEM as shown in **Figure 4.2**. It shows uncontrolled growth of nanowires along with forest of other nanostructures, irrespective of the presence of gold nanoparticles. The above experiment was repeated with reducing Ar flow to 50 sccm for 30 min after reaching set temperature to1160 ℃. Again, the gray-colored product so obtained on Si substrate was observed under SEM as shown in **Figure 4.3**. It shows gold catalysed condensation of ZnO randomly which cause ZnO growth by vapor – solid mechanism can be supported by hexagonal pattern at the tips of nanostructure.

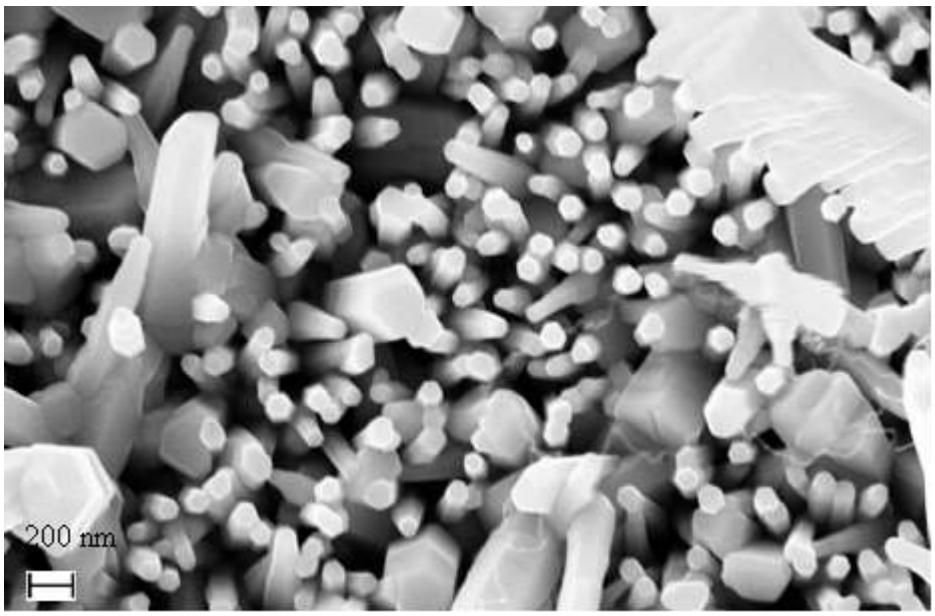

Figure 4.2 FESEM image of ZnO nanowires synthesized by VS technique. Weight of ZnO - 0.25 g. Weight of graphite – 0.25 g. Source temperature –1000 ℃ , subsrate temperature ~ 600 ℃ Argon flow rate – 200 sccm chamber pressure – 3.5 mbar. The image indicates uncontrolled growth of nanostructures irrespective of the presence of gold nanoparticles by vapour-solid mechanism.

In the present double-tube system, the argon flows from left to right in the large tube, whereas the Zn vapor flows in the opposite direction in the small tube. At the open end of the small tube, the tube vapors meet and oppose one another. Therefore, argon mainly flows up in the large tube, but the flow of ZnO vapor is blocked and forced to reverse its direction. As a result, vapor pressure of Zn above the substrate is high leading to rapid supersaturation followed by nanowires along with other nanostructures. At high Ar flow, vapor environment rate causes condensation of Zn vapor, no matter whether the substrate was coated with gold or not. In case of 50 sccm Ar flow rate, the vapor environment on substrate results in gold nanoparticle assisted ZnO condensation and hence the deposition of ZnO is random. It is anticipated that the present method should be applicable to the synthesis of well-aligned nanowire arrays. This is because the flow of carrier gas and ZnO vapor in the opposite direction

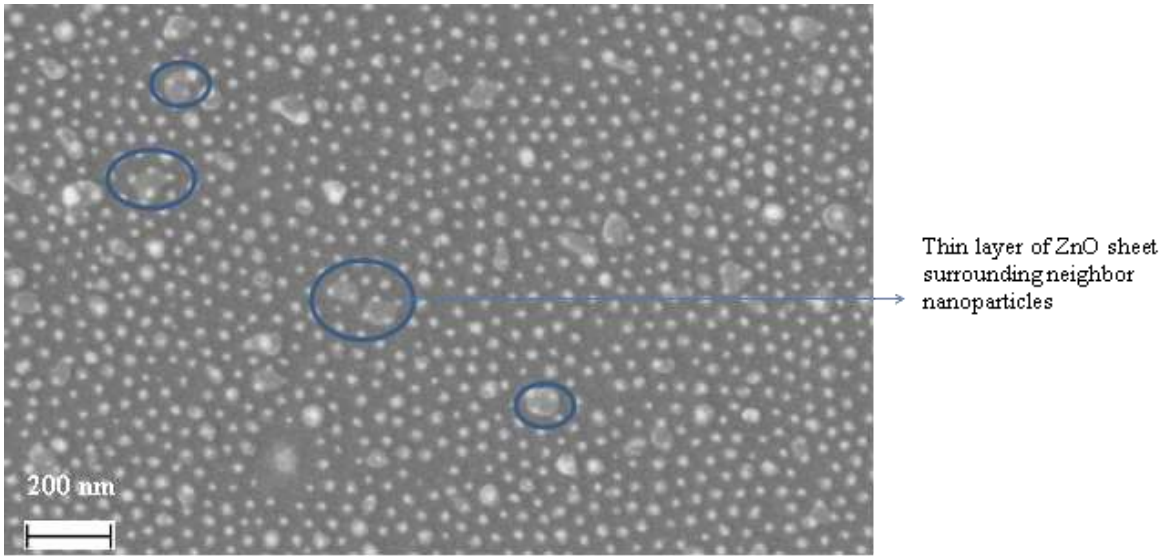

Figure 4.3 FESEM image of ZnO nanowires synthesized by VS technique. Weight of ZnO - 0.25 g. Weight of graphite – 0.25 g. Source temperature –1000 ℃, subsrate temperature ~ 600 ℃ Argon flow rate – 50 sccm chamber pressure – 3.5 mbar. The encircled section indicates the gold catalyzed condensation of ZnO randomly.

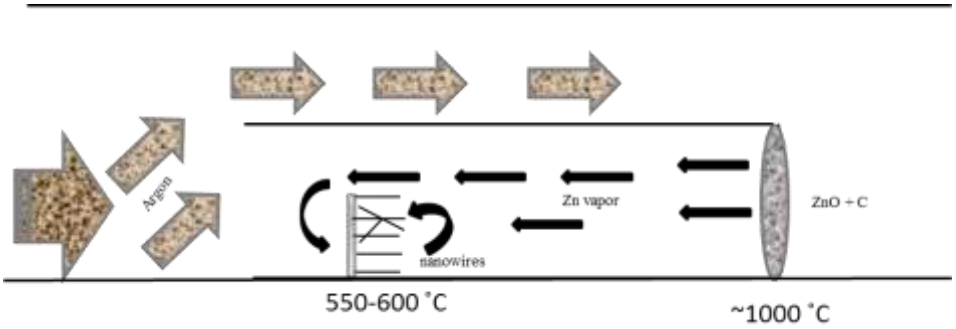

Figure 4.4 Vapor environment on the substrate forms relative balance and regional saturation to ensure the ZnO nanowire to be well aligned.

eventually forms a local balance and steady state which confine growth in the vertical direction[43]. A major weak point for double tube furnace is that the substrate temperature and substrate temperature cannot be easily varied. Temperature profile needs to be obtained again for any variation in source temperature due to close end of inner tube. Hereafter, the source and the substrate have been kept in alumina boat in typical tubular two zone furnace as shown in **Figure 4.5**.

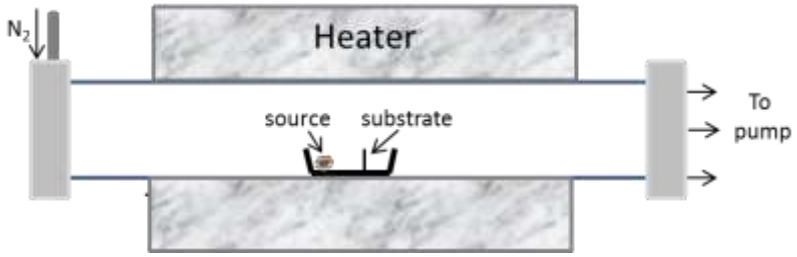

Figure 4.5 Schematic of the experimental setup of tubular furnace with source and substrate on alumina boat.

4.2 ZnO nanowire growth in a tubular furnace

A series of experiments were carried out on the growth of ZnO nanowire arrays using a physical vapour deposition process with Au as the catalyst and nitrogen as carrier gas. In order to identify the growth conditions that form well-aligned nanowires we have performed a study of the effects of various parameters that effect the growth. Specifically, we investigated the effects of the total pressure and ramping/cooling conditions on the diameter, density and structure of the nanowires. The standard experimental procedure mentioned in section 3.5.1 was followed in each experiment after baking the furnace. For consistency, all of the samples were collected at the 850 ℃ temperature zone, which is 3 cm away from the source material placed at 950 ℃.

4.2.1 Effect of the carrier gas

Two preliminary experiments were carried to justify the role of carrier gas in growth of ZnO nanowires. In first case, the experiment was done without supplying any carrier gas while the substrate was kept at 850 ℃ downstream to the source for 30 min. In second case, 100 sccm of N_2 gas was supplied for 5 min in the furnace when the substrate attained 850 ℃ . The pressure was sustained approximately 1 mbar in both cases for reaction. The SEM images have been shown in **Figure 4.6**. The role of carrier gas was also investigated at atmospheric conditions in similar way. The N_2 gas was supplied at 100 sccm for 10 min after rising of the substrate temperature to 850 ℃. The FESEM images shown in figure show nanostructures cannot be grown under atmospheric condition for given source and substrate temperature. Hence, we can impose atmospheric condition during cooling of the substrate to avoid unwanted deposition of Zn vapor. The results at low pressure can be explained by phase diagram shown in **Figure 2.4**.

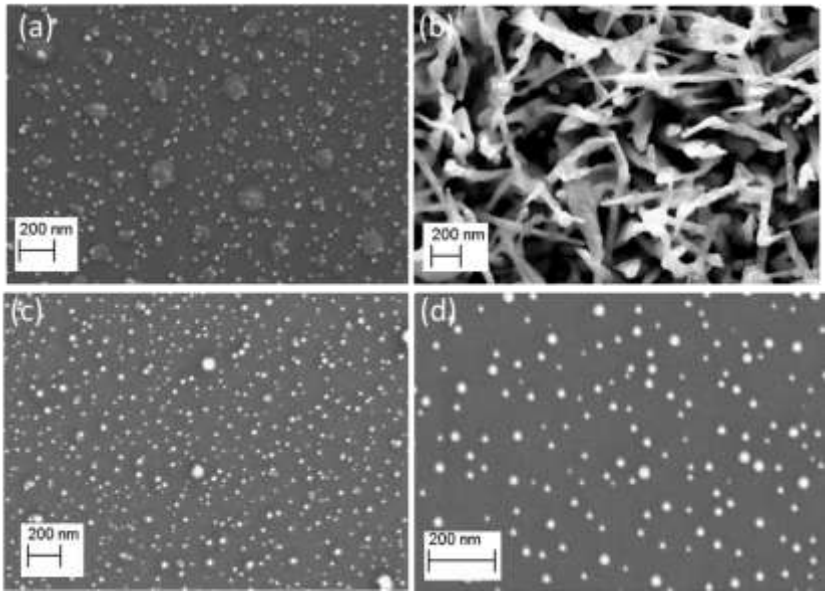

Figure 4.6 FESEM image showing the role of carrier gas at (a,b) 1 mbar and (c,d) 1 atm in VLS technique. The weight and temperature of source are 50 mg and 950 ℃ respecttively. The substrate temperature is 850 ℃ (a) N_2 gas was not supplied and the substrate was kept at 850 ℃ for 30 min. The pressure was set at 0.02 mbar during ramping and cooling of the furnace. (b) The substrate was sustained at 0.90 mbar under 100 sccm of N_2 gas for 5 min. The pressure was retained at 0.90 mbar

during ramping and cooling of the furnace. The substrate was maintained at 850 ℃ and 1 atm (c) without and (d) with N_2 gas for 10 min. The furnace was ramped up and cooled down under atmospheric condition.

4.2.2 Effect of the deposition temperature

Nanowires were grown at two different temperatures while keeping other parameters constant by changing the placement of the substrates downstream in the furnace. The SEM images of ZnO nanostructures grown at 800 ℃ and 850 ℃ at 19 mbar under N_2 flow rate of 100 sccm are shown in **Figure 4.7** and **Figure 4.8** . At high temperature, nanowires, nanobelts and triangular nanosheets were observed while shorter nanowires nuclei and nanothinfilm were seen at lower temperature. The result is supported by the work of Wongchoosuk et al[36]. The temperature affects the growth in two ways: it determines how much the Zn vapour would condense; and it also determines the length of the surface diffusion of the adsorbed vapour species. The surface diffusion of Zn atoms on Au nanoparticle is prominent at high substrate temperature resulting in nanowires growth with VLS mechanism. On the other hand, a high oxidation environment can also cause the growth of nanowires by VS mechanism. Hence, the governing growth mechanism becomes mixing structure between the VS and VLS mechanism and the shape becomes irregular. However, the surface diffusion length is much shorter than

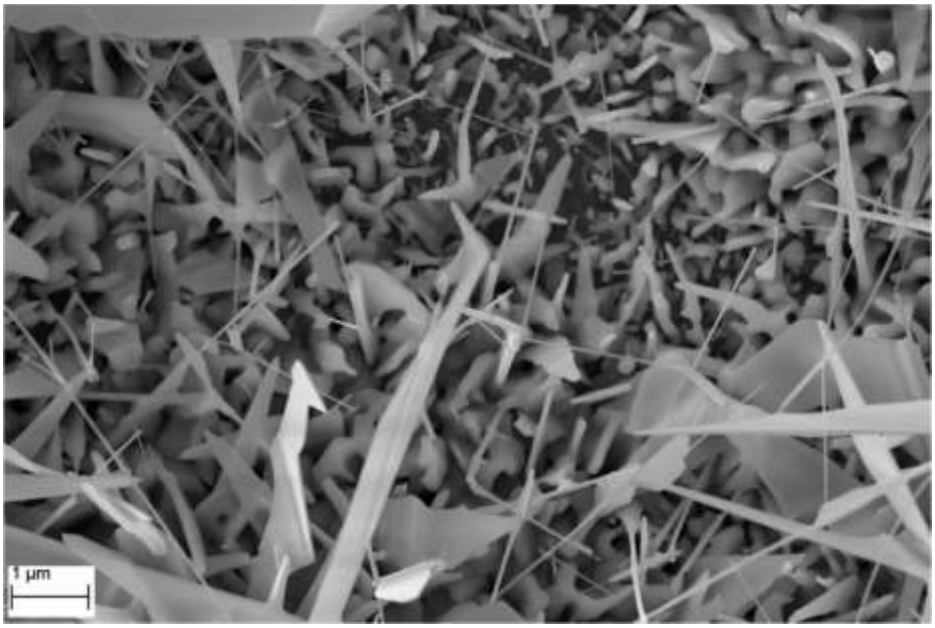

Figure 4.7 ZnO nanostructures grown using VLS and VS mechanism with substrate temperature at 850 ℃.

higher temperature, a large amount of Zn atoms cannot reach the preferential surface (c-surface for ZnO nanowires). Since the deposited Zn atoms would cause residual strain, they have to move to the other shortest direction to reduce the strain. In this case, ZnO nanowires expand in lateral direction at the sidewall and become wider, shorter and less dense compare to those grown at higher temperature.

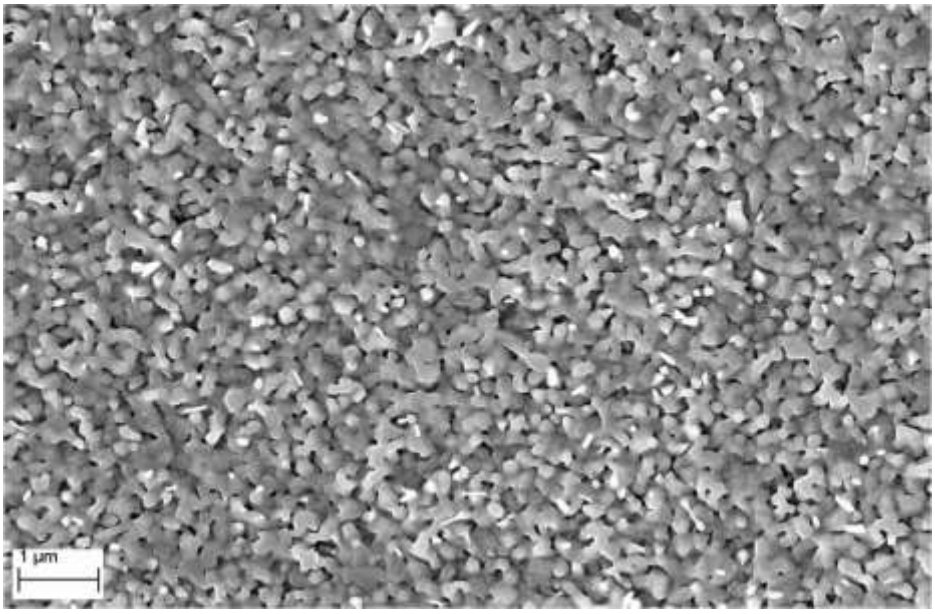

Figure 4.8 ZnO nanostructures grown using VLS and VS mechanism with substrate temperature at 800 ℃.

4.2.3 Effect of weight of the source

A set of experiments were performed to study the influence of weight of the source on grown nanostructures. The weight of source was varied from 250-50 mg while keeping other conditions constant. The pressure during ramping and cooling were maintained at 0.85 mbar, and 20 mbar during deposition of Zn vapor. The FESEM images are shown in **Figure 4.9**. The amount of source concerns with the amount of Zn vapor produced in the carbothermal reaction. Hence, higher amount of the source generates higher Zn vapor favouring rapid deposition by the VS as well as the VLS mechanism. However, the VS mechanism seems to be dominating in case of 250 mg weight of the source, as the gold nanoparticle could not be observed at tips of the nanostructures. With decrease in weight of the source, the VLS mechanism appears to be pronounced by virtue of catalyst at the tips. The triangular nanosheet is also found to be less dense owing to lower Zn vapor.

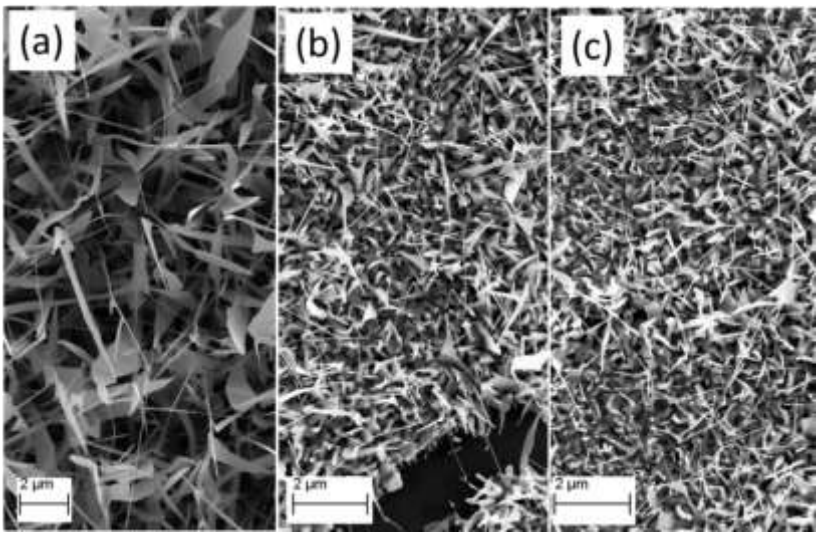

Figure 4.9 FESEM images of ZnO nanowires by VLS technique when weight of the source (mixture of ZnO and graphite in 1:1 ration by weight) is (a) 250mg, (b) 200 mg and (c) 50 mg. The source and the substrate were kept respectively at 950 ℃ and 850 ℃ for 10 min with 100 sccm N_2 flow rate.

4.2.4 Effect of the pressure condition

The pressure condition can be divided in to three intervals during an experiment:

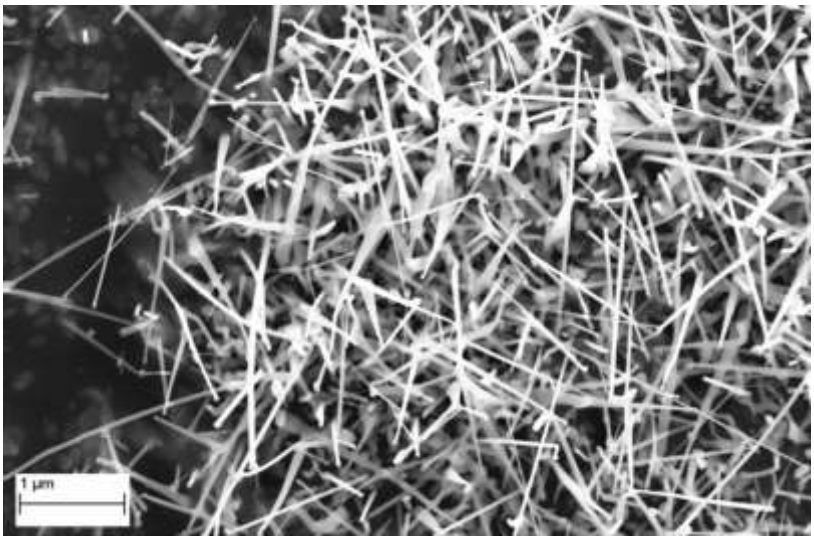

Figure 4.10 FESEM image of ZnO nanowires grown by VLS mechanism. The pressure was maintained at 0.89 mbar during ramping, deposition and cooling of the furnace under 100 sccm flow rate of N_2 gas. The weight of source was 50 mg and it was kept at 850 ℃ for 15 min.

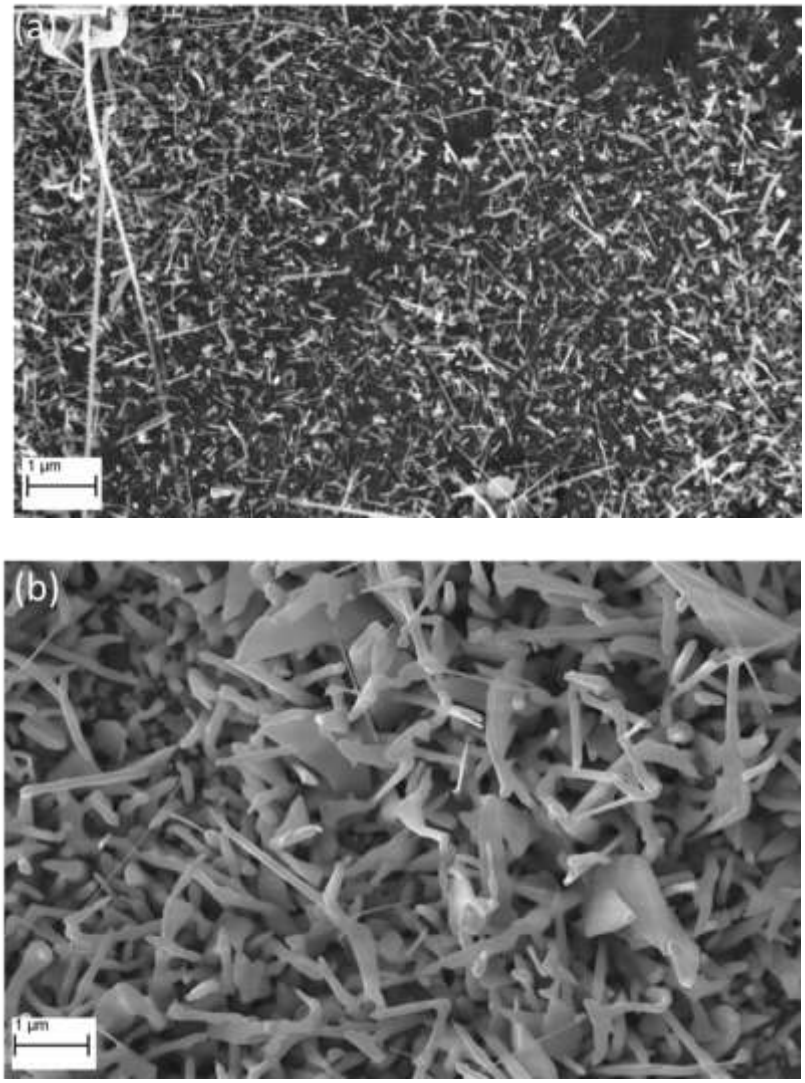

Figure 4.11 FESEM images of ZnO nanowires grown by VLS mechanism. The pressure was maintained at (a) 1.1 mbar and (b) 5 mbar during ramping, deposition and cooling of the furnace under 200 sccm flow rate of Ar gas. The weight of source was 250 mg and kept at 850 ℃ for 15 min.

ramping pressure, the pressure while the temperature is ramping; deposition pressure, when Zn vapor is supposed to condense on Au nanoparticles to grow nanowires; and cooling pressure, the substrate is allowed to cool inside furnace after deposition. The deposition pressure seems to have the most dramatic effect in changing the morphology of the wires. In **Figure 4.10** and **Figure 4.11**, the SEM image of samples is shown in which the pressure was maintained at 0.89, 1.1 and 5 mbar during the experiment.

In a couple of samples, the ramping pressure was kept at 0.88 mbar while deposition pressure was uphold at 19 mbar and 27 mbar. The deposition and cooling pressure were retained same. The FESEM images are shown in **Figure 4.12**.

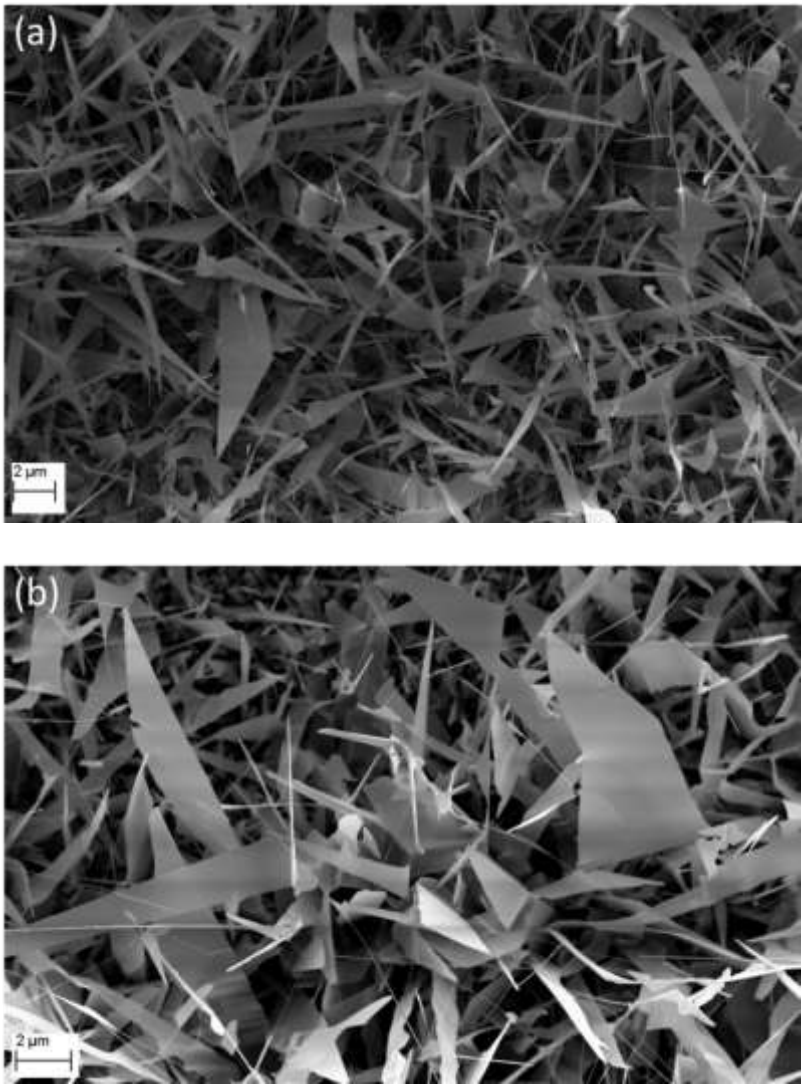

Figure 4.12 FESEM images of ZnO nanowires grown by VLS mechanism. The ramping pressure was maintained at 0.88 mbar. The pressure was kept at (a) 19 mbar and (b) 27 mbar during deposition as well as cooling of the furnace under 100 sccm flow rate of Ar gas. The weight of source was 250 mg and kept at 850 ℃ for 15 min.

In following set of samples, the ramping was preserved at 0.84 mbar. The deposition pressure was kept at 13, 20 and 65 mbar whereas the cooling pressure was done at 1 atm, 0.84 mbar and 1 atm respectively. The atmospheric pressure was imposed to check the unwanted deposition of Zn vapour during cooling. The FESEM images of nanostructures shown in **Figure 4.13** suggest that undesirable deposition leading to heterogeneous structures may occur during ramping period.

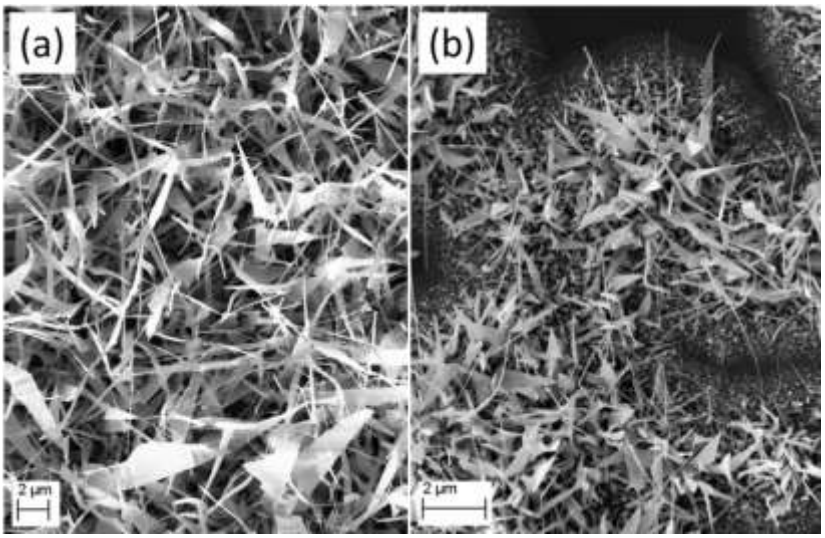

Figure 4.13 FESEM images of ZnO nanostructures by VLS mechanism. The ramping and cooling pressure were kept same in both samples at 0.84 mbar and 1 atm. The deposition pressure was maintained at (a) 13 mbar and (b) 65 mbar for 10 min. The weight of source was (a) 250 mg and (b) 200 mg. The source and substrate temperature were $950℃$ and $850℃$ respectively.

Varying the deposition pressure changes not only the diameter, length and density of the wires but also the morphology of the nanostructures that are grown. In most of the samples, apart from nanowires, nanobelts and planes, nanowires with forks, and flexible nanobelts, and triangular nanosheets are formed. The supersaturation level of the zinc vapor is critical to determining the type of growth that occurs. It seems to be higher at low pressures and decreases at higher pressures. This could be because more powder was evaporated at low pressures, creating more vapour.

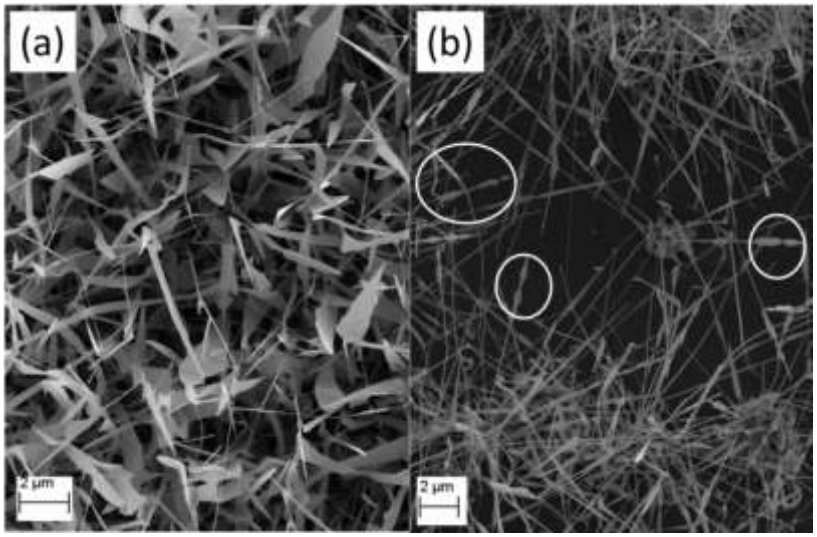

Figure 4.14 FESEM images of ZnO nanowires grown at 20 mbar for 10 min by VLS technique at two different location of the same sample. Both ramping and cooling pressure were preserved at 0.84 mbar. The weight of source was 200 mg. The source and substrate temperature were $950℃$ and $850℃$ respectively. The white solid circles in left image mark existence of dripping and condensation of Zn-Au alloy on nanowires during cooling period.

At low pressures, higher supersaturation also leads to secondary nucleation and different type of growth as the environment is far away from thermal equilibrium. According to Ye at al[44], this non-equilibrium kinetic growth may create a low-surface-energy tip which allows molecules to diffuse away easily to energetic side surfaces causing the growth of nanobelts and sheets and platelets. For higher pressures the supersaturation may be low, allowing anisotropic growth at an energetic nanowire tip but no nucleation on the sides. The globular structure can be observed on nanowires in **Figure 4.14b**. It implies dripping followed by condensing of Zn-Au droplets during cooling period. The substrate cannot be isolated during ramping and cooling periods in the present experimental setup which cause undesirable deposition of Zn vapor leading to growth of various heterogeneous nanostructures. These nanostructures can also be seen in almost all samples. The formation of irreproducible nanostructures can also be attributed to switching of pressure from ramping to deposition or deposition to cooling condition. During transition of pressure, the substrate is exposed to a gradient of pressure and may cause nuclei formation by the VS or VLS mechanism randomly. As the diameter of wires decreases, the length increases because of the smaller amount of vapor needed to grow thinner wires.

5 Summary

A method has been developed to process degraded thiol-terminated polystyrene to obtain self-assembly of gold nanoparticle arrays following work of Muralidharan et al[25]. The thermal stable nanoparticle array so obtained was used as catalyst to grow ZnO nanowires by vapor-liquid-solid technique. The experiments were done in a typical tubular furnace as well as double-tube furnace. The process conditions for the growth of vertically aligned ZnO nanowires were studied as a function of the carrier gas, the weight of the source powder and the deposition temperature. The carrier gas is necessary for transport of vapor to the metal catalyst. The high weight of source generates high Zn vapor and intensifies the VS mechanism to grow nanowires. The lower temperature favours formation of nanowire nuclei or nanosheets while higher temperature leads to thinner and longer nanowires. The significance of ramping, deposition and cooling pressures were investigated extensively and found to be crucial. The unwanted condensation of Zn vapor before and after deposition period has resulted in various heterogeneous structures like triangular nanosheets, nanowires with forks, nanoribbons, nanobelts and planes in addition to nanowires. The growth appears to be occurring through both mechanisms together: the vapour-liquid-solid technique and the vapour solid technique. However, the growth of nanosturctures seems to be assisted by gold nanoparticles on every sample as no deposition was observed beyond the horizon of self-assembly nanoparticle arrays on the substrates.

6 Future work

The present experimental setup needs to be modified to facilitate the following: to control experiments at different deposition pressure, and to limit the exposure of the substrates to experimental conditions only during deposition period. The shutter approach may be incorporated

to resolve this issue. Under this approach, the source and the substrate can be kept in zone 1 and zone 2 respectively as shown in **Figure 6.1**.

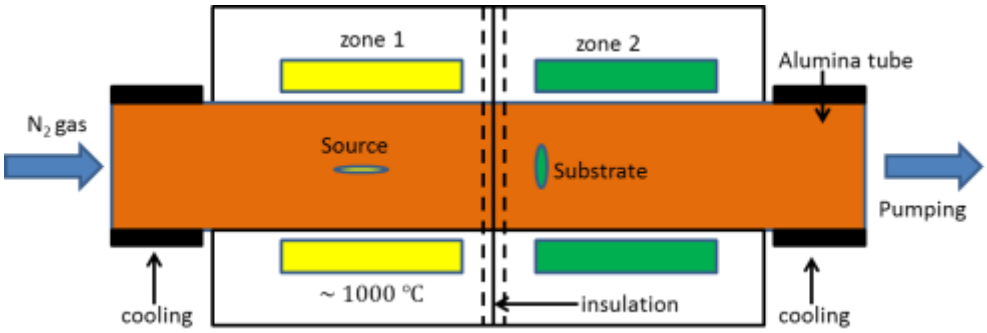

Figure 6.1 Schematic diagram of the two zone heating furnace with pressure shutter method.

It enables to control the source and substrate environment separately and hence can be used to prevent the unwanted growth of ZnO nanowires during the temperature ramping and cooling. After loading the sample and evacuating the tube, the temperature can be ramped from the room temperature to a desired temperature. During the ramping, the pressure can be set to 1 atm. The pressure is not suitable for a ZnO nanowire growth and there is no deposition. After the source temperature reaches the set point, the pressure is set and maintained for reaction for 10 min at desired scale. Then, the furnace is cooled down and pressure is set to 1 bar again with continuous supply of carrier gas.

In addition, the experimental parameters should be tailored in order to achieve proper vapor environments needed for the growth of vertically nanowire array. Experiments should be carried to study controllable growth of vertical zinc oxide nanowires with a focus on effect of the catalyst size and distribution, total pressure and the partial pressure of oxygen on the diameter, density and structure of nanowires. Zinc powder can also be used as source to investigate the growth of ZnO nanowires. Finally, performance of DSSC will be tested by measuring internal quantum efficiencies of devices made using the grown nanowires as photoanodes.

References

1. Crabtree GW, Lewis NS. Solar energy conversion. *Physics Today.* 2007;60(3):37-42.

2. Grätzel M. Solar energy conversion by dye-sensitized photovoltaic cells. *Inorganic Chemistry.* 2005;44(20):6841-6851.

3. Lewis NS. Powering the planet. *MRS Bulletin.* 2007;32(10):808-820.

4. Chiba Y, Islam A, Watanabe Y, Komiya R, Koide N, Han L. Dye-Sensitized Solar Cells with Conversion Efficiency of 11.1%. *Japanese Journal of Applied Physics.*45:L638-L640.

5. O'Regan B, Grätzel M. A low-cost, high-efficiency solar cell based on dye-sensitized colloidal TiO2 films. *Nature.* 1991;353(6346):737-740.

6. Shockley W, Queisser HJ. Detailed balance limit of efficiency of p-n junction solar cells. *Journal of Applied Physics.* 1961;32(3):510-519.

7. Baxter JB, Aydil ES. Nanowire-based dye-sensitized solar cells. *Applied Physics Letters.* 2005;86(5):1-3.

8. Law M, Greene LE, Johnson JC, Saykally R, Yang P. Nanowire dye-sensitized solar cells. *Nature Materials.* 2005;4(6):455-459.

9. Coakley KM, McGehee MD. Conjugated polymer photovoltaic cells. *Chemistry of Materials.* 2004;16(23):4533-4542.

10. Gonzalez-Valls I, Lira-Cantu M. Vertically-aligned nanostructures of ZnO for excitonic solar cells: A review. *Energy and Environmental Science.* 2009;2(1):19-34.

11. Nazeeruddin MK, Péchy P, Renouard T, et al. Engineering of efficient panchromatic sensitizers for nanocrystalline TiO 2-based solar cells. *Journal of the American Chemical Society.* 2001;123(8):1613-1624.

12. Benkstein KD, Kopidakis N, Van de Lagemaat J, Frank AJ. Influence of the percolation network geometry on electron transport in dye-sensitized titanium dioxide solar cells. *Journal of Physical Chemistry B.* 2003;107(31):7759-7767.

13. Huang SY, Schlichthörl G, Nozik AJ, Grätzel M, Frank AJ. Charge recombination in dye-sensitized nanocrystalline TiO2 solar cells. *Journal of Physical Chemistry B.* 1997;101(14):2576-2582.

14. Peter LM, Wijayantha KGU. Electron transport and back reaction in dye sensitized nanocrystalline photovoltaic cells. *Electrochimica Acta.* 2000;45(28):4543-4551.

15. Martinson ABF, McGarrah JE, Parpia MOK, Hupp JT. Dynamics of charge transport and recombination in ZnO nanorod array dye-sensitized solar cells. *Physical Chemistry Chemical Physics.* 2006;8(40):4655-4659.

16. Galoppini E, Rochford J, Chen H, et al. Fast electron transport in metal organic vapor deposition grown dye-sensitized ZnO nanorod solar cells. *Journal of Physical Chemistry B.* 2006;110(33):16139-16161.

17. Baxter JB, Walker AM, Van Ommering K, Aydil ES. Synthesis and characterization of ZnO nanowires and their integration into dye-sensitized solar cells. *Nanotechnology.* 2006;17(11):S304-S312.

18. Greene LE, Law M, Goldberger J, et al. Low-temperature wafer-scale production of ZnO nanowire arrays. *Angewandte Chemie - International Edition.* 2003;42(26):3031-3034.

19. Sivaraman SK, Kumar S, Santhanam V. Room-temperature synthesis of gold nanoparticles - Size-control by slow addition. *Gold Bulletin.* 2010;43(4):275-286.

20. Mårtensson T, Borgström M, Seifert W, Ohlsson BJ, Samuelson L. Fabrication of individually seeded nanowire arrays by vapour–liquid–solid growth. *Nanotechnology.* 2003;14(12):1255.

21. Ng HT, Han J, Yamada T, Nguyen P, Chen YP, Meyyappan M. Single crystal nanowire vertical surround-gate field-effect transistor. *Nano Letters.* 2004;4(7):1247-1252.

22. Mårtensson T, Carlberg P, Borgström M, Montelius L, Seifert W, Samuelson L. Nanowire arrays defined by nanoimprint lithography. *Nano Letters.* 2004;4(4):699-702.

23. Greyson EC, Babayan Y, Odom TW. Directed growth of ordered arrays of small-diameter ZnO nanowires. *Advanced Materials.* 2004;16(15 SPEC. ISS.):1348-1352.

24. Hong Jin F, Woo L, Roland S, et al. Arrays of vertically aligned and hexagonally arranged ZnO nanowires: a new template-directed approach. *Nanotechnology.* 2005;16(6):913.

25. Muralidharan G, Sivaraman SK, Santhanam V. Effect of substrate on particle arrangement in arrays formed by self-assembly of polymer grafted nanoparticles. *Nanoscale.* 2011;3(5):2138-2141.

26. Hochbaum AI, Yang P. Semiconductor nanowires for energy conversion. *Chemical Reviews.* 2010;110(1):527-546.

27. Law M, Goldberger J, Yang P. Semiconductor nanowires and nanotubes. Vol 342004:83-122.

28. Schmidt V, Wittemann JV, Gösele U. Growth, thermodynamics, and electrical properties of silicon nanowires. *Chemical Reviews.* 2010;110(1):361-388.

29. Fan HJ, Werner P, Zacharias M. Semiconductor nanowires: From self-organization to patterned growth. *Small.* 2006;2(6):700-717.

30. Garnett EC, Brongersma ML, Cui Y, McGehee MD. Nanowire solar cells. Vol 412011:269-295.

31. Wacaser BA, Dick KA, Johansson J, Borgström MT, Deppert K, Samuelson L. Preferential interface nucleation: An expansion of the VLS growth mechanism for nanowires. *Advanced Materials.* 2009;21(2):153-165.

32. Okamoto H. Au-Zn (Gold-Zinc). *Journal of Phase Equilibria and Diffusion.* 2006;27(4):427-427.

33. Zacharias M, Subannajui K, Menzel A, Yang Y. ZnO nanowire arrays – Pattern generation, growth and applications. *physica status solidi (b).* 2010;247(10):2305-2314.

34. Pung SY, Choy KL, Hou X. Tip-growth mode and base-growth mode of Au-catalyzed zinc oxide nanowires using chemical vapor deposition technique. *Journal of Crystal Growth.* 2010;312(14):2049-2055.

35. Kim DS, Scholz R, Gösele U, Zacharias M. Gold at the root or at the Tip of ZnO Nanowires: A Model. *Small.* 2008;4(10):1615-1619.

36. Wongchoosuk C, Subannajui K, Menzel A, et al. Controlled Synthesis of ZnO Nanostructures: The Role of Source and Substrate Temperatures. *The Journal of Physical Chemistry C.* 2011/01/27 2010;115(3):757-761.

37. Dalal SH, Baptista DL, Teo KBK, Lacerda RG, Jefferson DA, Milne WI. Controllable growth of vertically aligned zinc oxide nanowires using vapour deposition. *Nanotechnology.* 2006;17(19):4811.

38. Song, WangWang, Riedo E, Wang ZL. Systematic Study on Experimental Conditions for Large-Scale Growth of Aligned ZnO Nanwires on Nitrides. *The Journal of Physical Chemistry B.* 2005/05/01 2005;109(20):9869-9872.

39. Ramgir NS, Subannajui K, Yang Y, Grimm R, Michiels R, Zacharias M. Reactive VLS and the Reversible Switching between VS and VLS Growth Modes for ZnO Nanowire Growth. *The Journal of Physical Chemistry C.* 2010/06/17 2010;114(23):10323-10329.

40. Kodambaka S, Tersoff J, Reuter MC, Ross FM. Germanium nanowire growth below the eutectic temperature. *Science.* 2007;316(5825):729-732.

41. Cleland WW. Dithiothreitol, a new protective reagent for SH groups. *Biochemistry.* 1964;3(4):480-482.

42. Tsarevsky NV, Matyjaszewski K. Reversible redox cleavage/coupling of polystyrene with disulfide or thiol groups prepared by atom transfer radical polymerization. *Macromolecules.* 2002;35(24):9009-9014.

43. Geng C, Jiang Y, Yao Y, et al. Well-Aligned ZnO Nanowire Arrays Fabricated on Silicon Substrates. *Advanced Functional Materials.* 2004;14(6):589-594.

44. Ye C, Fang X, Hao Y, Teng X, Zhang L. Zinc Oxide Nanostructures: Morphology Derivation and Evolution. *The Journal of Physical Chemistry B.* 2005/10/01 2005;109(42):19758-19765.